Ji Desheng Snake Pill activate p53 signaling pathway promotes GPX4-mediated Ferroptosis to exert anti-hepatocellular carcinoma effects

Journal:	*Science Progress*
Manuscript ID	SCI-25-1703
Manuscript Type:	Original Research Article
Date Submitted by the Author:	23-Jul-2025
Complete List of Authors:	Li, Hui; Jiangsu Province Academy of Traditional Chinese Medicine Zhang, Xuan; Nantong University Affiliated Hospital Yang, Hui; The Central Hospital of Wuhan Yuan, Hui; Nanjing Hospital of Chinese Medicine Affiliated to Nanjing University of Chinese Medicine Wu, Fan; Jiangnan University Xue, Boyu; Jiangsu Province Academy of Traditional Chinese Medicine,
Keywords:	Ji Desheng Snake Pill, p53 signaling pathway, RNA-Seq, Ferroptosis, Hepatocellular carcinoma
Abstract:	BACKGROUND: Ji Desheng Snake Pill (JDS) has been used in the clinic as an adjuvant therapy for patients with hepatocellular carcinoma (HCC), its active ingredient and potential drug mechanism have not yet been clarified. Ferroptosis is a metabolic cell death putative dependent on ferric ions, and the process is closely related to tumour development. OBJECTIVE: To explore the potential drug mechanism of anti-tumour action of JDS and the correlation between JDS and Ferroptosis. MATERIALS AND METHODS: Tumour xenograft animal model was constructed by in vivo experiments and HepG2 cell culture in vitro to observe the anti-tumour drug effects after JDS intervention. Combined with transcriptomics to explore the drug action mechanism of JDS exerting anti-tumour effects. RESULTS: In the in vivo experiments, We found that JDS significantly increased the level of ferritin deposition in subcutaneous grafted tumors and attenuated cell proliferation, thereby delaying tumor progression. In vitro, we found that JDS drug serum significantly reduced the migration and growth of HepG2 cells, and promoted the accumulation of lipid peroxides and induced Ferroptosis, and then we found that the main mechanism of JDS was closely related to p53 and other related pathways by transcriptomics sequencing. Finally, a retrospective study revealed that inhibition of p53 pathway activation could reduce the promotion of Ferroptosis by JDS. CONCLUSION: The present study demonstrated that JDS could promote the accumulation of lipid peroxides by activating the p53 signaling pathway, and induced Ferroptosis in HCC cells, which significantly reduced the proliferation of HCC cells.

Ji Desheng Snake Pill activate p53 signaling pathway promotes GPX4-mediated Ferroptosis to exert anti-hepatocellular carcinoma effects

Hui Li [1, 2#], Xuan Zhang [3], Qingchun Yang [4], Xin Yuan [5], Fan Wu [6], Boyu Xue [1*]

[1] Affiliated Hospital of Nanjing University of Chinese Medicine, Jiangsu Provincial Hospital of Traditional Chinese Medicine, Nanjing, China.

[2] Rugao Hospital Affiliated to Nantong University, Nantong, China.

[3] Affiliated Hospital of Nantong University, Nantong, China.

[4] The Central Hospital of Wuhan, Tongji Medical College, Huazhong University of Science and Technology, Wuhan, China.

[5] Nanjing Hospital of Traditional Chinese Medicine, Nanjing, China.

[6] Department of Hepatopancreatobiliary Surgery， Jiangnan University Affiliated Central Hospital， Wuxi, China

*** Correspondence:**

Boyu Xue, Department of general medicine, Affiliated Hospital of Nanjing University of Chinese Medicine, Jiangsu Provincial Hospital of Traditional Chinese Medicine, No.155 Hanzhong Road, Qinhuai District, Nanjing, Jiangsu, China

Email: huili9696@163.com

TEL: 86-13809037933

Abstract

BACKGROUND: Ji Desheng Snake Pill (JDS) has been used in the clinic as an adjuvant therapy for patients with hepatocellular carcinoma (HCC), its active ingredient and potential drug mechanism have not yet been clarified. Ferroptosis is a metabolic cell death putative dependent on ferric ions, and the process is closely related to tumour development.

OBJECTIVE: To explore the potential drug mechanism of anti-tumour action of JDS and the correlation between JDS and Ferroptosis.

MATERIALS AND METHODS: Tumour xenograft animal model was constructed by in vivo experiments and HepG2 cell culture in vitro to observe the anti-tumour drug effects after JDS intervention. Combined with transcriptomics to explore the drug action mechanism of JDS exerting anti-tumour effects.

RESULTS: In the in vivo experiments, We found that JDS significantly increased the level of ferritin deposition in subcutaneous grafted tumors and attenuated cell proliferation, thereby delaying tumor progression. In vitro, we found that JDS drug serum significantly reduced the migration and growth of HepG2 cells, and promoted the accumulation of lipid peroxides and induced Ferroptosis, and then we found that the main mechanism of JDS was closely related to p53 and other related pathways by transcriptomics sequencing. Finally, a retrospective study revealed that inhibition of p53 pathway activation could reduce the promotion of Ferroptosis by JDS.

CONCLUSION: The present study demonstrated that JDS could promote the accumulation of lipid peroxides by activating the p53 signaling pathway, and induced Ferroptosis in HCC cells, which significantly reduced the proliferation of HCC cells.

Keywords

Ji Desheng Snake Pill; p53 signaling pathway; RNA-Seq; Ferroptosis; Hepatocellular carcinoma;

Graphical Abstract

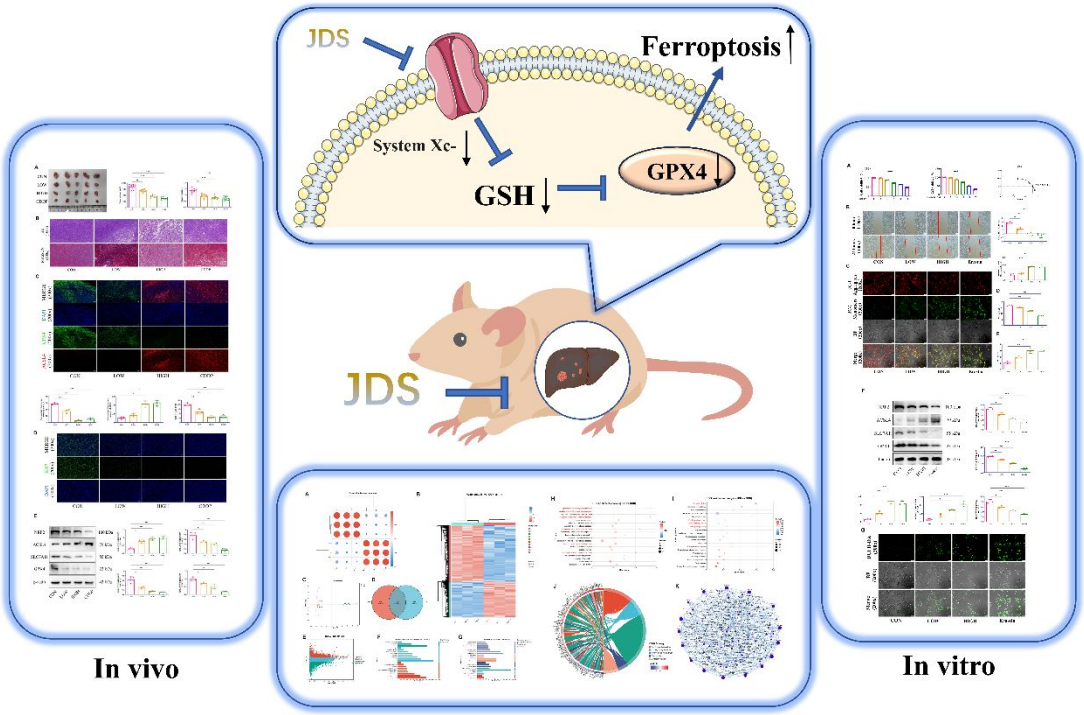

Introduction

Hepatocellular carcinoma (HCC) is a high-mortality primary liver cancer, and as one of the most common malignancies, it is the third leading cause of cancer-related deaths[1] .HCC has been found to be highly associated with risk factors such as genetics, hepatitis, and obesity[2]. Safer, effective and non-invasive therapeutic strategies are still the focus of HCC research.

Ferroptosis, an emerging type of programmed cell death, is caused by iron-dependent lipid peroxidation, which results from a combination of aberrant cellular metabolism and an imbalance in redox homeostasis[3]. Many metabolic disorders are strongly associated with this process. Ferroptosis has also been implicated as a key mechanism in the regulation of cancer in a variety of cancers[4-6]. In the field of liver cancer, researchers have found that Ferroptosis plays an important role in the treatment of HCC[7]. One of the non-coding RNAs (ncRNAs) has the ability to control iron concentration in HCC cells, thereby affecting disease progression and drug resistance in tumours[8]. Clinically, sorafenib, a first-line drug for the treatment of hepatocellular carcinoma, exhibits a strong Ferroptosis effect[9]. Therefore, the development of drugs targeting Ferroptosis for the treatment of HCC has great potential for development.

Many traditional Chinese medicines and their active ingredients have shown better anti-tumour effects, and compared with traditional western medicines, traditional Chinese medicines have the advantages of less toxic side effects and a wide range of safe concentrations[10,11]. Ji Desheng Snake Pill (JDS) was developed based on the empirical formula of Mr. Ji Desheng, a famous traditional Chinese medicine practitioner in Jiangsu Province, and clinical studies in recent years have shown that it has achieved certain clinical efficacy in the treatment of hepatocellular carcinoma, and it has a great potential to be developed into an anti-tumour drug targeting Ferroptosis[12,13]. Polyphyllin, as the main active ingredient of Chonglou, has been found to inhibit breast cancer progression by inhibiting the PI3K/AKT

pathway[14]. In colorectal cancer research, Polyphyllin can inhibit the Notch pathway to prevent cancer cell growth[15]. In HCC, Polyphyllin has been found to activate the ZBTB16/PPARγ/RXRα signaling axis to treat liver cancer[16]. In Ferroptosis, Polyphyllin can promote the accumulation of lipid peroxides through PI3K/SREBP-1/SCD1 signaling axis to cause Ferroptosis[17]. Therefore, further in-depth investigation of the drug mechanism of action of JDS will help to discover new ways to treat HCC.

Therefore, the potential anti-tumour drug action mechanism of JDS has not yet been clarified, and the link between JDS and Ferroptosis deserves to be explored in depth. The aim of this study was to investigate the link between JDS and Ferroptosis and the specific mechanism of action by which it exerts anti-tumour effects.

Methods and Materials

Main Reagents and Drugs

Ji Desheng Snake Pill is sourced from commercialized products manufactured by Jinghua Pharmaceutical Group Co., Ltd., under the production approval by National Medical Products Administration of China (National Medicine Permission Number Z32020048). Nrf2 (1:1,000, HY-P81051, MCE, USA), GPX4 (1:1,000, 67763-1-Ig, Proteintech, China), ACSL4 (1:1,000, 22401-1-AP, Proteintech, China), SLC7A11 (1:1,000, FNab10533, FineTest, China), p53 (1:1,000, 60283-2-Ig, Proteintech, China), p21 (1:1,000, HY-P80773, MCE, USA), MDM2 (1:1,000, CSB-PA156585, Cusabio, China), MDM4 (1:1,000, CSB-PA013627GA01HU, Cusabio, China) and GAPDH (1:1,000, 60004-1-Ig, Proteintech, China).

Animal cell group culture and intervention

Seventy 5-week-old BALB/C male nude mice were purchased from Jiangsu Huachuang Xinnuo Company. The animal experiment was approved by the Animal Ethics Committee of Jiangnan University (JN. No20240830b0250228). The concentration of HepG2 cells was adjusted to 1 × 107/mL, and 0.1 mL of cell suspension was inoculated into each of 40 nude mice. Tumour volume was measured using vernier calipers, and group pharmacological interventions were started when the tumour volume reached 100 mm3. Using statistical software, the animals were randomly divided into the following groups: blank control group (saline group), low concentration of Ji Desheng Snake Pill (JDS) group (25 mg/kg/d), high concentration of JDS Snake Drug group (50 mg/kg/d), and cisplatin (CDDP) group (25 mg/kg/d). All nude mice were executed after anaesthesia, and tumour blocks were taken to measure their length and width, and their volume and weight were calculated.

UPLC-Q-TOF-HRMS

The configured JDS drug solution was analyzed and assayed using Ultra-high-performance liquid chromatography-quadrupole-time-of-flight-high-resolution mass spectrometry (UPLC-Q-TOF-HRMS) for compositional analysis and detection. The detection conditions were as follows: Liquid phase:18 Liquid mobile phase: waters BEH C18 column (1.7μm, 2.1*50mm); Mobile phase: A: 0.1% formic acid; B: 0.1% formic acid acetonitrile; Gradient elution: (0–2min, 95%A, 5%B; 2–30min, 95%-2%A, 5%-98%B; 30–35 min, 2%A, 98%B; 35–39 min, 2%-95% A, 98%-5% B; 39~40min, 95%A, 5%B); Flow rate: 0.4mL/min column temperature: 40°C; The detection volume was 3μL. The detection conditions of the positive mode of mass spectrometry were as follows: nitrogen flow rate 800L/h; Voltage 2kv; Desolvation temperature 400°C; The ion source temperature was 110°C. Collision voltage 20–40V; The collection mass number ranged from 50 to 1200. The detection condition of the negative electric mode of mass spectrometry was 1.5kv, and the other setting conditions were the same as those of the positive electric mode.

Histopathology

Tissue wax blocks were made from the transplanted tumour and sectioned. Sections were soaked in xylene, gradient dehydrated, stained with hematoxylin-eosin dye solution on tissue sections and then soaked in distilled water and washed, again gradient dehydrated with ethanol, transparent with xylene for 20 minutes, then neutral gel was added to seal the sections and the tissue changes were observed under light microscope. Tissue immunofluorescence The sections were permeabilised with 0.3% Triton x-100 for 20 minutes. After sealing with 5% BSA for 1 h, the sections were incubated with primary antibody at 4 °C overnight. The next day the sections were incubated for 1 h with secondary antibody with fluorescent labelling. Sections were blocked using an anti-fluorescence quenching blocking solution containing DAPI. Final images were obtained on a laser microscope.

HepG2 cell group culture and intervention

HepG2 cells were gifted by Fang Fei's group at Jiangnan University. HepG2 cells were cultured in DMEM medium (Gibco, item no.: C11965500BT) containing 10% FBS (Gibco, item no.: 10099141) in an incubator at 37℃ with 5% CO2. SD rats were dosed with JDS drug in order to extract JDS drug serum for pharmacological intervention on HepG2 cells, where 5% JDS drug serum was used in the low concentration JDS group and 10% JDS drug serum was used in the high concentration JDS group.

CCK-8 assay

HepG2 cells were seeded in 96-well plates at a density of 3x103 cells/well, and after the cells were adhered to the wall and grew, the medium was configured with different concentrations (0, 2%, 4%, 6%, 8%, 10%) of JDS drug serum, and the medium was configured with different concentrations (0, 5, 10, 15, 20, 25 μmol/L) of Erastin (MCE, item no.: HY-15763).) in the medium, respectively, and after 24 h of intervention, configured CCK-8 working solution (APExBIO, item no.: K1018) was added to each well and incubated at 37 °C for 2 h. The medium was then incubated for 2 h at 37 °C for 2 h at 37 °C. The OD value (absorbance) was detected at 450 nm.

Cellular scarring

The six-well plate was pre-marked with a marker pen, and HepG2 cells were inoculated in the six-well plate at a density of 5 × 105 cells/well. After the cells had grown adherently and fused to 90% of the area, a 200 μl pipette tip was used to make a cut along the centre of the well plate perpendicular to the marking line of the marker pen, and then rinsed carefully three times with PBS to remove cell debris. The growth status and migration of labelled cells in each well were photographed using an inverted light microscope at the time points of 0 and 24 h of incubation. Image migration distances were analysed using ImageJ software and the migration rate (MR) was calculated.MR (%) = (24 h scratch distance/0 h scratch

distance) x100.

JC-1

According to the experimental protocol provided by the reagent vendor, the JC-1 Mitochondrial Membrane Potential Detection Kit (C2003, Beyotime, China) was used to load the in situ probe on the intervened chondrocytes, and the working solution was configured and then incubated with the cells for 20 min at 37°C environment, and washed by PBS, and then observed under the fluorescence inverted microscope and pictures were collected.

WB

HepG2 cells and tumour tissues were lysed and proteins were extracted using RIPA lysis buffer (Thermo Scientific, item number: 89901). Sample protein concentrations were determined using a NanoDrop microspectrophotometer (Thermo Scientific). 20 μg of sample per group was used and separated by 10% SDS-PAGE and then transferred to a PVDF membrane. After sealing with 5% skimmed milk for 2 h at room temperature, the membranes, after washing using TBST, were then incubated with primary antibodies at 4 °C overnight. The next day the membranes were washed and incubated with the secondary antibody with HRP at room temperature for 1 hour at room temperature. The luminescence intensity was subsequently detected on a chemiluminescence imager (ImageQuant LAS 4000mini) using the ECL Substrate Kit (Tanon, item no. 180-506), and the expression levels of the relevant proteins were determined by calculating the bands with ImageJ software.

ROS

According to the experimental protocol provided by the reagent vendor, the intervened chondrocytes were loaded with in situ probes using the ROS assay kit ROS assay (Dojindo, R252), and the working solution was configured and incubated with the cells for 20 min at 37°C, washed with

PBS, and then observed under a fluorescence inverted microscope and pictures were collected.

Glutathione (GSH) Assay

According to the experimental protocol provided by the reagent vendor, the intervened chondrocytes were loaded with in situ probes using the ROS assay kit ROS assay (Dojindo, R252), and the working solution was configured and incubated with the cells for 20 min at 37°C, washed with PBS, and then observed under a fluorescence inverted microscope and pictures were collected.

Malondialdehyde (MDA) assay

Cells were collected and pooled with EP tubes as required in the kit instructions (Jiancheng, A003-1). After 500 μL of extract was added to the tubes, the cells were repeatedly broken by ultrasonic waves for 30 times, and then divided into EP tubes, the supernatant was collected and placed on ice, and 300 μL of malondialdehyde working solution, 100 μL of distilled water, and 100 μL of malondialdehyde reagent were added, respectively. A water bath at 100 °C for 120 min was used and immediately placed on ice for cooling process, centrifuged again and appropriate amount of supernatant was aspirated and placed in a 96-well plate, and the OD value of each well was tested by an enzyme marker. The OD value of each well was measured by an enzyme marker and brought into the formula to calculate the amount of MDA in the samples to be tested.

Transcriptomics and data analysis

The transcriptomes of the control and high JDS concentration groups were determined using the Illumina NovaSeq 6000. Each group had 3 independent replicates for a total of 6 samples. Quality control of raw reads and adapter trimming was done using fastp (v 0.20.0). High quality reads were retained and used for further downstream analysis using a quality Phred score cutoff of 30. Transcripts were quantified using RSEM. Transcribed nucleotide sequences were searched and annotated against the protein database

by running BLAST (blastx). Differential expression analysis was performed using the DESeq2R software package and principal component analysis (PCA) was performed on each sample based on expression. Transcripts with log2foldChange > = 2 and p-value < = 0.05 were considered significantly up-regulated in the differential analysis, and transcripts with log2foldChange < = -2 and p-value < = 0.05 were considered significantly down-regulated. Gene ontology (GO) enrichment analysis based on differentially expressed genes and Kyoto Encyclopedia of Genes and Genomes (KEGG) pathway were performed in Cytoscape.

Statistical analysis

All data are shown as mean and standard deviation (SD), and all experiments were guaranteed to be tested three or more times in independent experiments. Data between groups were statistically analysed and plotted in GraphPad Prism 8.0 using the unpaired two-tailed Student's t-test.

Results

1. The Therapeutic Component in JDS

After the UPLC-Q-TOF-HRMS results were examined, we found that the main components in JDS include 49 active ingredients, which mainly include phenolic acids, flavonoids, alkaloids and steroids (Supplementary table 1). Thirty-seven components were identified in cationic mode (Fig.1A), which mainly contained Diosmetin 7-O-rutinoside, Swertisin, 5-Methoxyfurfural, etc. Twelve components were identified in anionic mode (Fig.1B), which mainly contained Ethylparaben, Chrysoeriol-7-O-rutinoside, 4-Hydroxybenzoate and other components.

2. JDS inhibits xenograft tumour growth in vivo

Low and high concentrations of JDS and cisplatin were used to intervene in nude mice transplanted with HepG2 cells, respectively, in order to observe and compare the antitumour drug effects of JDS. The results showed that the volume and weight of the transplanted tumours were significantly reduced after intervention with low concentration of JDS, high concentration of JDS and cisplatin compared to the blank control group (Fig.2A). Meanwhile, the histopathological staining results combined with Ki67 fluorescence staining showed that the cell density in the transplanted tumour was reduced, the number of proliferating cells was reduced after the intervention of low concentration of JDS, high concentration of JDS and cisplatin (Fig.2B,C). And by fluorescent labelling of GPX4 and ASCL4 proteins (Fig.2D), we found that the expression level of GPX4 protein in the transplanted tumour was decreased and the expression level of ACSL4 protein was increased after the intervention of low concentration of JDS, high concentration of JDS and cisplatin. To quantify the expression levels of Ferroptosis-related proteins within the transplanted tumour in a single step, we used WB to detect the protein expression levels of

NRF2, ASCL4, SLC7A11 and GPX4 in the transplanted tumour (Fig.2E). The results showed that JDS was able to promote the expression level of ASCL4 protein, reduce the protein expression level of NRF2, SLC7A11 and GPX4, and exacerbate the level of Ferroptosis in the transplanted tumour, and the anti-tumour effect of JDS showed a drug concentration gradient.

3. JDS promotes GPX4-mediated Ferroptosis process to inhibit HepG2 cell proliferation

Firstly, we screened and determined the optimal intervention concentrations of JDS drug serum and Erastin on HepG2 cells by CCK-8 assay. The results showed (Fig.3A) that when the intervention time was 24h, JDS drug serum greater than 6% significantly reduced the proliferation viability of HepG2 cells; meanwhile, when Erastin was 20 μM, it significantly reduced the proliferation viability of HepG2 cells, and the IC50 of Erastin was 19.67 μM.In order to determine whether JDS drug serum played an inhibitory role in the proliferation of HepG2 cells, we determined the optimal concentration of JDS drug serum by performing the CCK-8 assay on HepG2 cells in each group. proliferation, we performed cell scratch assay on each group of HepG2 cells, and the results showed (Fig.3B) that the proliferation efficiency and migration rate of HepG2 cells were decreased after the intervention of low concentration of JDS drug serum, high concentration of JDS drug serum, and Erastin, compared with the control group in 24 h. The results showed that the proliferation efficiency and migration rate of HepG2 cells were decreased after the intervention of low concentration of JDS drug serum, high concentration of JDS drug serum, and Erastin, compared with the control group. The Ferroptosis process was closely linked to the state of oxidative stress, and ROS accumulation was closely related to the state of mitochondria. By observing the degree of ROS accumulation and changes in mitochondrial membrane potential levels in HepG2 cells in each group (Fig.3C,G), we found that low concentration of JDS drug serum, high

concentration of JDS drug serum, and Erastin intervention were enough to promote the accumulation of ROS and the decrease of membrane potential in HepG2 cells. And by detecting GSH and MDA content in HepG2 cells in each group, the results showed (Fig.3D,E) that low concentration of JDS drug serum, high concentration of JDS drug serum and Erastin interventions promoted the level of MDA content and reduced the level of GSH content. Meanwhile, in order to quantify the expression levels of Ferroptosis-related proteins in transplanted tumours as soon as possible, we used WB to detect the protein expression levels of NRF2, ASCL4, SLC7A11, and GPX4 in HepG2 cells in each group (Fig.3F). The results showed that JDS was able to promote the expression level of ASCL4 protein and reduce the protein expression level of NRF2, SLC7A11 and GPX4, and the results of the in vitro experiments were consistent with those in the in vivo experiments.

4. JDS promotes Ferroptosis reversal of the protective effect of Fer-1 in HepG2 cells

In order to further verify the effect of Ferroptosis on HepG2 cells, the pharmacological effect of JDS on HepG2 cells was determined after the intervention of HepG2 cells using Fer-1, an Ferroptosis inhibitor. WB detected the protein expression levels of NRF2, ASCL4, SLC7A11, and GPX4 in the HepG2 cells of each group, and the results showed that (Fig.4A), Fer -1 intervention promoted the protein expression levels of NRF2, SLC7A11 and GPX4, and decreased the protein expression level of ASCL4; the intervention with JDS drug serum was able to reverse the effect of Fer-1 on HepG2 cells, and JDS decreased the protein expression levels of NRF2, SLC7A11 and GPX4, and increased the protein expression level of ASCL4, which promotes the the production of Ferroptosis process in HepG2 cells. By performing cell scratch assay on HepG2 cells in each group, the results showed (Fig.4B) that compared with the control group, Fer-1 intervention promoted the migration of HepG2 cells; while JDS

drug serum intervention was able to reverse the effect of Fer-1 on HepG2 cells and inhibit the migration of HepG2 cells. Meanwhile, the results of JC-1 and ROS also showed that (Fig.4C,D), compared with the control group, there was no difference between the degree of accumulation of ROS and the level of mitochondrial membrane potential in HepG2 cells after the intervention of Fer-1; whereas, the intervention of JDS drug serum exacerbated the degree of accumulation of ROS, and led to the decrease in the level of mitochondrial membrane potential. Similarly, the detection of MDA and GSH content in HepG2 cells in each group showed that there was no difference in the levels of MDA and GSH content in HepG2 cells after Fer-1 intervention, whereas JDS drug serum intervention promoted the levels of MDA content and decreased the levels of GSH content in HepG2 cells(Fig.4E,F).

5. Transcriptomic analyses targeting the interventional effects of JDS on HepG2 cells

In order to further explore the potential mechanism of drug action exerted by JDS snake drug against hepatocellular carcinoma cells, HepG2 cells from the blank control group and the high concentration of JDS drug serum group were collected for RNA-Seq, and the correlation analysis between the samples showed that (Fig.5A), there was a significant difference in the transcriptional level of the HepG2 cells in the blank control group and the HepG2 cells after the intervention of the JDS drug serum. The PCA analysis of the results also further confirmed that there were differences in gene expression between the two groups after down-regulation (Fig.5B).Venn diagram analysis of the number of differential genes between the two groups showed (Fig.5C) that the number of genes co-expressed in the two groups was 13,047 genes, whereas 1,506 uniquely expressed genes existed in the blank group, and 395 uniquely expressed genes were expressed after the JDS intervention. Through differential gene clustering analysis heatmap display we found that there was a significant difference between the two groups (Fig.5D). By

volcano scatter plot we can find that 1349 gene expression levels were up-regulated and 2086 gene expression levels were down-regulated after JDS intervention (Fig.5E). Annotation analysis of the differential genes by using GO database showed that they were mainly concentrated in the terms of protein binding, cellular components and cellular processes (Fig.5F). The most obvious changes after annotation analysis of differential genes by using KEGG database focused on Signal transduction (Fig.5G). The results of GO enrichment analysis showed (Fig. 5H) that the words related to lipid metabolism, such as regulation of sterol biosynthetic process, regulation of cholesterol biosynthetic process, regulation of cholesterol metabolic process, and regulation of lipid biosynthetic process pathway, underwent a bright change after JDS intervention. These results suggest that JDS is closely related to lipid metabolism process in the process of anti-HCC. The results of enrichment analysis using KEGG showed (Fig.5I) that circadian rhythm, steroid biosynthesis, FoxO signaling pathway, MAPK signaling pathway, p53 signaling pathway and Ferroptosis were significantly altered in response to JDS intervention. Further addressing the relationship between the differential genes and the KEGG pathway was demonstrated by enrichment analysis of chordal plots (Fig. 5J), which showed that the intervention of JDS promoted the expression of related genes, such as SAT1, MAP1LC3B2, and ALOX15, and lowered the expression level of the SLC7A11 gene, which promotes the Ferroptosis process. Meanwhile, JDS was also in the upstream and downstream pathways closely related to Ferroptosis, such as p53 signaling pathway, MAPK signaling pathway and FoxO signaling pathway. Finally, the protein interaction network analysis diagram (Fig.5K) was drawn to demonstrate the potential connection between differential genes.

6. JDS promotes Ferroptosis by activating the p53 signaling pathway

In order to validate the results of RNA-Seq, we intervened HepG2 cells with JDS and the p53 inhibitor PFT-α to further explore the drug action mechanism of JDS. The results of WB showed (Fig.6A) that compared with the blank group, the protein expression levels of p53,p21 were significantly increased in HepG2 cells after JDS intervention, and those of MDM2 and MDM4 were levels were significantly reduced; at the same time, p53,p21 protein expression levels were reduced and MDM2 and MDM4 protein expression levels were increased in HepG2 cells after PFT-α intervention; whereas, compared to the JDS group, p53,p21 protein expression levels were increased and MDM2 and MDM4 protein expression levels were reduced in HepG2 cells after co-intervention of JDS and PFT-α. After we found by mitochondrial membrane potential, GSH and MDA assay (Fig.6B-D), compared with the blank group, the mitochondrial membrane potential level decreased, GSH level decreased, and MDA content increased after JDS intervention; and compared with the PFT-α group, the same manifestations were observed in the HepG2 cells after the co-intervention of JDS and PFT-α. The results of Ferroptosis-related protein expression content of the cells in each group showed (Fig.6E) that compared with the blank group, the protein expression level of ACSL4 was significantly increased in HepG2 cells after JDS intervention, and the protein expression levels of NRF2, GPX4 and SLC7A11 were significantly decreased; meanwhile, the protein expression level of ACSL4 in HepG2 cells after PFT-α intervention was decreased, and the protein expression levels of NRF2, GPX4 and SLC7A11 increased; whereas, compared with the JDS group, the protein expression levels of ACSL4 in HepG2 cells were decreased, and the protein expression levels of NRF2, GPX4 and SLC7A11 increased after the co-intervention of JDS and PFT-α, and the PFT-α intervention attenuated the effect of JDS on Ferroptosis. We further observed the mitochondrial morphology by electron microscopy to determine the oxidative stress damage in HepG2 cells (Fig.6F), and the results showed that the mitochondrial morphology in the tumour cells

in the control group was relatively intact, presenting an elongated strip, with the internal mitochondrial cristae morphology intact; the mitochondria of the tumour cells appeared to have obvious morphological changes after the intervention of JDS, presenting an elliptical and round shape, with the disappearance of the internal cristae morphology of the mitochondria, and the mitochondrial damage was serious; the mitochondrial damage was severe after the co-intervention of JDS and The mitochondrial morphology was improved after the co-intervention of JDS and PFT-α, and the drug effect of JDS was attenuated by PFT-α.

7. PFT-α intervention attenuates the effect of JDS on xenograft tumour Ferroptosis

To further validate the conclusions drawn from the in vitro experiments, we used xenograft tumours to observe the effect of PFT-α intervention on the antitumor efficacy of JDS. The anti-tumour efficacy was initially judged by recording the weight and volume of the xenograft tumours in each group, and the results showed (Fig.7A) that the volume and weight of the xenograft tumours were significantly reduced after JDS intervention compared to the blank control group, and the volume and weight of the xenograft tumours were increased after the co-intervention of JDS and PFT-α compared to the JDS group. And the number of Ki67-positive cells in the transplanted tumours in each group was observed by immunofluorescence, and the results showed (Fig.7B) that the number of Ki67-positive cells in the transplanted tumours was significantly reduced after the intervention with JDS compared to the blank control group; and the number of Ki67-positive cells in the transplanted tumours was increased after the co-intervention of JDS and PFT-α relative to the JDS group. The results of pathological staining also showed (Fig.7C) that the cell density within the transplanted tumour was reduced after JDS intervention compared to the blank group; whereas the PFT-α intervention attenuated the drug effect of JDS raising

the cell density within the transplanted tumour. We used WB to observe the expression levels of p53 signaling pathway and Ferroptosis-related proteins in the transplanted tumours of each group, and the results showed (Fig.7D) that JDS intervention increased the protein expression levels of p53, p21 and ASCL4 in the transplanted tumours, and decreased the protein expression levels of MDM2, MDM4, NRF2, SLC7A11, and GPX4; while PFT-α intervention attenuated the drug effects produced by JDS, reduced the protein expression levels of p53, p21 and ASCL4 in the transplanted tumour, and increased the protein expression levels of MDM2, MDM4, NRF2, SLC7A11 and GPX4. We thus concluded that the p53 inhibitor PFT-α could reduce the anti-tumour effect produced by JDS because it inhibited the activation of p53 by JDS and attenuated the Ferroptosis-promoting effect of JDS.

Discussion

The global prevalence of hepatic cell carcinoma (HCC) is increasing year by year, and HCC is still a worldwide health problem[18]. With the advancement of medical science and technology, various kinds of treatments for HCC are emerging[19]. Currently, the main treatments for liver cancer include surgery, chemotherapy, targeted therapy, immunotherapy, etc. However, these treatments can only slow down the disease progression of HCC, and are still very helpful to the patients. However, these treatments can only slow down the progression of HCC, and their help to patients is still very limited, so it is very necessary to find more effective and safe treatments with less side effects.

In the field of antitumour therapy, more and more traditional Chinese medicines have been explored by researchers and have achieved great potential in clinical treatment and improved the quality of life of cancer patients[20]. JDS has been gradually and innovatively applied in various disease areas and achieved certain efficacy in anticancer therapy[21-23]. The active ingredients contained in JDS, such as Chonglou and Di Jin Cao, have been deeply studied in various tumour treatment fields[10,24]. Among them, Chonglou mainly contains steroidal saponins such as Chonglou saponin I, Chonglou saponin II and Chonglou saponin III[10]. Dijinzhao mainly contains flavonoids such as kaempferol, quercetin and scopolamine. Most of these components have been found to have some anticancer effects in research[24]. In the treatment of liver cancer, kaempferol can inhibit the cell cycle by regulating the ATM/CHEK2/KNL1 pathway in hepatocellular carcinoma cells, thus exerting antitumour drug effects[25]. Quercetin can slow down the progression of hepatocellular carcinoma by inhibiting vesicles secreted by vascular endothelial cells[26].

p53 is a widely studied oncogene that is closely associated with the cell cycle and carcinogenesis, and relevant studies have reported mutations and inactivation of the p53 gene in typically more than 50% of cancer patients[27]. In the field of hepatocellular carcinoma, activation of p53 promotes the expression

of the downstream protein p21, and researchers have found that by degrading the p21 protein promotes cell proliferation and increases oncogenic potential[28]. In a similar study, degradation of p53 expression by the ubiquitinating enzyme MARCH5 would further exacerbate the progression of HCC[29]. Our study showed that JDS intervention significantly increased the protein expression of p53 and p21 and delayed HCC.

At the same time, we showed that p53 is closely related to Ferroptosis sensitivity. p53 can transcriptionally inhibit SLC7A11, which is the subunit of System x- and is responsible for the transporter activity of the main antioxidant system[30]. Inhibition of System xc- inhibits cystine uptake, inhibits GSH synthesis, and leads to a decrease in the activity of the enzyme GPX4, which leads to a decrease in the activity of the enzyme GPX4[31]. Inhibition of System xc- activity inhibits cystine uptake and GSH synthesis, which in turn leads to a decrease in the activity of the membrane lipid repair enzyme GPX4, which reduces the antioxidant capacity of the cells and induces Ferroptosis in tumour cells[32]. On the other hand, activation of p53 affects the phospholipase iPLA2β, which promotes the production of lipid peroxides and MDA, and accelerates Ferroptosis[33]. The results of transcriptomics showed that the p53 signaling pathway was significantly activated by JDS intervention, which significantly reduced the transcript levels of p53 antagonism-related MDM-2 and MDM-4, and consequently increased the p53 transcript levels in cancer cells. Thus p53 plays a key role in Ferroptosis. Our study found that JDS acts on the p53 signaling pathway and promotes the protein expression level of p53 to reduce SLC7A11 synthesis, leading to abnormal intracellular antioxidant function and reduced GSH level, promoting the production of MDA and the impairment of mitochondrial function, which effectively reduces Ferroptosis antagonism exerted by GPX4, and ultimately leads to the emergence of tumour cell Ferroptosis.

Although our study preliminarily explored the potential of JDS as a novel inducer targeting Ferroptosis and the mechanism of drug action it exerts. However, JDS, as a pharmaceutical compound composed of multiple Chinese medicines, the small molecule compounds that exert specific drug effects still need to be further identified and discussed in depth. In the future, multidisciplinary collaboration between clinical medicine, biochemistry and materials science needs to be actively pursued to further extract the effective drug components within JDS, and optimisation of the innovative preparation process will be more helpful in the search for the discovery of effective measures for the treatment of HCC.

In summary, firstly, we found that JDS can promote the accumulation of lipid peroxides and facilitate the Ferroptosis process to improve tumour progression. Through the use of transcriptomics technology and the combination of in vivo and in vitro experiments, we found that JDS inhibits tumour growth by activating the p53 signaling pathway and exerts Ferroptosis-promoting drug effects. In conclusion, JDS plays an anti-tumour role by activating the p53 signaling pathway, aggravating the accumulation of lipid peroxides and promoting the Ferroptosis process.

Declarations

Clinical trial number

Not applicable.

Consent for publication

The authors declare that the research was conducted in the absence of any commercial or financial relationships that could be construed as a potential conflict of interest.

Availability of data and material

All results and data are maintained in the Department of general medicine, Affiliated Hospital of Nanjing University of Chinese Medicine, Jiangsu Provincial Hospital of Traditional Chinese Medicine. Data will be made available from the corresponding author on reasonable request.

Funding

This research was supported by the Nantong Infectious Disease Alliance Research Project. (No. 202308008)

Declaration of interest statement

The authors declare that they have no known competing financial interests or personal relationships that could have appeared to influence the work reported in this paper.

Authors' contributions

Hui Li: Writing – original draft, Funding acquisition.

Xuan Zhang: Resources, Methodology.

Qingchun Yang: Resources, Data curation.

Xin Yuan: Investigation.

Fan Wu: Formal analysis, Data curation.

Boyu Xue: Writing – review & editing.

Abbreviations

JDS(Ji Desheng Snake Pill)

HCC (hepatocellular carcinoma)

CDDP (cisplatin)

DMEM(Dulbecco's Modified Eagle Medium)

FBS(Fetal bovine serum)

BSA(Bovine Serum Albumin)

DAPI(2- (4-Amidinophenyl)-6-indolecarbamidine dihydrochloride)

CCK-8(Cell Counting Kit-8)

MR(migration rate)

ROS(reactive oxygen species)

MDA(Malondialdehyde)

REFERENCES

(1) Tang, D.; Kroemer, G.; Kang, R. Ferroptosis in hepatocellular carcinoma: from bench to bedside. *Hepatology*. **2024**, *80*(3), 721-739, DOI: 10.1097/HEP.0000000000000390.

(2) Chen, X.; Kang, R.; Kroemer, G.; Tang, D. Broadening horizons: the role of ferroptosis in cancer. *Nat. Rev. Clin. Oncol.* **2021**, *18*(5), 280-296, DOI: 10.1038/s41571-020-00462-0.

(3) Li, S.; Zhang, G.; Hu, J.; Tian, Y.; Fu, X. Ferroptosis at the nexus of metabolism and metabolic diseases. *Theranostics* **2024**, *14*(15), 5826-5852, DOI: 10.7150/thno.100080.

(4) Elsakka, E.; Midan, H. M.; Abulsoud, A. I.; Fathi, D.; Abdelmaksoud, N. M.; Abdel, M. S.; Zaki, M. B.; Abd-Elmawla, M. A.; Rizk, N. I.; Elrebehy, M. A.; et al. Emerging insights: mirna modulation of ferroptosis pathways in lung cancer. *Exp. Cell Res.* **2024**, 114272, DOI: 10.1016/j.yexcr.2024.114272.

(5) Tang, L.; He, D.; Su, B. Nrf2: a critical participant in regulation of apoptosis, ferroptosis, and autophagy in gastric cancer. *Acta Histochem.* **2024**, *126*(8), 152203, DOI: 10.1016/j.acthis.2024.152203.

(6) Wang, Y.; Cao, X.; Yang, C.; Fan, J.; Zhang, X.; Wu, X.; Guo, W.; Sun, S.; Liu, M.; Zhang, L.; et al. Ferroptosis and immunosenescence in colorectal cancer. *Semin. Cancer. Biol.* **2024**, *106-107*, 156-165, DOI: 10.1016/j.semcancer.2024.10.003.

(7) Wang, P.; Kong, G. Comprehensive analysis of angiogenesis and ferroptosis genes for predicting the survival outcome and immunotherapy response of hepatocellular carcinoma. *J. Hepatocell. Carcinoma* **2024**, *11*, 1845-1859, DOI: 10.2147/JHC.S483647.

(8) Liu, B.; Liu, L.; Liu, Y. Targeting cell death mechanisms: the potential of autophagy and ferroptosis in hepatocellular carcinoma therapy. *Front. Immunol.* **2024**, *15*, 1450487, DOI: 10.3389/fimmu.2024.1450487.

(9) Jiang, Y.; Yu, Y.; Pan, Z.; Glandorff, C.; Sun, M. Ferroptosis: a new hunter of hepatocellular carcinoma. *Cell Death Discov.* **2024**, *10*(1), 136, DOI: 10.1038/s41420-024-01863-1.

(10) Ke, F.; Zhang, R.; Chen, R.; Guo, X.; Song, C.; Gao, X.; Zeng, F.; Liu, Q. The role of rhizoma paridis saponins on anti-cancer: the potential mechanism and molecular targets. *Heliyon* **2024**, *10*(17), e37323, DOI: 10.1016/j.heliyon.2024.e37323.

(11) Wang, L.; Huang, H.; Li, X.; Ouyang, L.; Wei, X.; Xie, J.; Liu, D.; Tan, P.; Hu, Z. A review on the research progress of traditional chinese medicine with anti-cancer effect targeting ferroptosis. *Chin. Med.* **2023**, *18*(1), 132, DOI: 10.1186/s13020-023-00838-1.

(12) Ni Xuejiao; Xu Chunming; Xu Aibing; Xu Hu; Gu Yishu; Wei Guohua; Ji Jinfeng; Yang Yang Observations on the clinical effect of Ji Desheng snake medicine combined with chemotherapy in the treatment of primary hepatocellular carcinoma. *Journal of Practical Clinical Medicine* **2019**, 23(24), 61-63.[In Chinese]

(13) Zhang Yu; Gao Qian; Shao Jianguo; Da Kunlin; Chen Yufeng; Weng Jiaxin; Chen Lin Clinical efficacy of Ji Desheng's snake medicine in the treatment of patients with middle- to late-stage hepatocellular carcinoma of the damp-heat and stasis type and its effect on patients' serum mir-335. *Chinese Journal of Integrative Medicine and Digestion* **2022**, 30(06), 411-418. [In Chinese]

(14) Miao, W.; Wang, Z.; Gao, J.; Ohno, Y. Polyphyllin ii inhibits breast cancer cell proliferation via

the pi3k/akt signaling pathway. *Mol. Med. Rep.* **2024**, *30*(6), DOI: 10.3892/mmr.2024.13348.
(15) Wang, Y.; Ge, H.; Zhang, Y.; Wang, P.; Zhao, H.; Wang, L.; Fan, Z. Antitumor effect of polyphyllin i (ppi) on colorectal cancer: evidence from patient-derived organoids and notch signaling suppression. *Heliyon* **2024**, *10*(18), e37226, DOI: 10.1016/j.heliyon.2024.e37226.
(16) Shan, L.; Chen, Y.; An, G.; Tao, X.; Qiao, C.; Chen, M.; Li, J.; Lin, R.; Wu, J.; Zhao, C. Polyphyllin i exerts anti-hepatocellular carcinoma activity by targeting zbtb16 to activate the ppar γ /rxr α signaling pathway. *Chin. Med.* **2024**, *19*(1), 113, DOI: 10.1186/s13020-024-00984-0.
(17) Zhou, X.; Zhang, D.; Lei, J.; Ren, J.; Yang, B.; Cao, Z.; Guo, C.; Li, Y. Polyphyllin i induces rapid ferroptosis in acute myeloid leukemia through simultaneous targeting pi3k/srebp-1/scd1 axis and triggering of lipid peroxidation. *J. Nat. Med.* **2024**, *78*(3), 618-632, DOI: 10.1007/s11418-024-01811-4.
(18) Danpanichkul, P.; Suparan, K.; Prasitsumrit, V.; Ahmed, A.; Wijarnpreecha, K.; Kim, D. Long-term outcomes and risk modifiers of masld between lean and non-lean populations. *Clin. Mol. Hepatol.* **2024**, DOI: 10.3350/cmh.2024.0631.
(19) Stefanini, B.; Manfredi, G. F.; D'Alessio, A.; Fulgenzi, C.; Awosika, N.; Celsa, C.; Pirisi, M.; Rigamonti, C.; Burlone, M.; Vincenzi, F.; et al. Delivering adjuvant and neoadjuvant treatments in the early stages of hepatocellular carcinoma. *Expert Rev. Gastroenterol. Hepatol.* **2024**, 1-14, DOI: 10.1080/17474124.2024.2419519.
(20) Ruishi, X.; Linyi, X.; Yunfan, B.; Wenbo, Y.; Xiaoying, Z.; Xiaoxue, F.; Difu, Z.; Xintian, L.; Ming, Z.; Haoming, L. New perspectives on chemokines in hepatocellular carcinoma therapy: a critical pathway for natural products regulation of the tumor microenvironment. *Front. Immunol.* **2024**, *15*, 1456405, DOI: 10.3389/fimmu.2024.1456405.
(21) Tan, L. L.; Huang, Y.; Liang, X. Y.; Huo, L.; Lu, Y. H. Thunder fire moxibustion combined with external application of Ji, D. S. snake medicine for the treatment of diabetes mellitus combined with herpes zoster: a clinical study. *Guangxi Traditional Chinese Medicine* **2023**, 46(02), 30-33. [In Chinese]
(22) Yao,Y Clinical observation on 32 cases of mumps in children treated with external application of snake medicine by Ji Desheng. *Chinese Community Physician* **2021**, 37(03), 131-132. [In Chinese]
(23) Ye L; He W. Effects of antivenom combined with Ji Desheng snake medicine on the degree of swelling and coagulation function after venomous snake bite. *Snake Journal* **2023**, 35(04), 431-434. [In Chinese]
(24) Rakotondrabe, T. F.; Fan, M.; Hu, G.; Guo, M. Potential hemostatic compounds targeting urokinase plasminogen activator explored from three euphorbiaceae species: euphorbia maculata, euphorbia humifusa, and acalypha australis, with bio-affinity ultrafiltration uplc-ms. *Phytochem. Anal.* **2024**, *35*(1), 28-39, DOI: 10.1002/pca.3270.
(25) Li, X.; Zhou, M.; Zhu, Z.; Wang, Z.; Zhang, X.; Lu, L.; Xie, Z.; Wang, B.; Pan, Y.; Zhang, J.; et al. Kaempferol from alpinia officinarum hance induces g2/m cell cycle arrest in hepatocellular carcinoma cells by regulating the atm/chek2/knl1 pathway. *J. Ethnopharmacol.* **2024**, *333*, 118430, DOI: 10.1016/j.jep.2024.118430.
(26) Reyes-Avendaño, I.; Reyes-Jiménez, E.; González-García, K.; Pérez-Figueroa, D. C.; Baltiérrez-Hoyos, R.; Tapia-Pastrana, G.; Sánchez-Chino, X. M.; Villa-Treviño, S.; Arellanes-Robledo, J.; Vásquez-Garzón, V. R. Quercetin regulates key components of the cellular microenvironment during early hepatocarcinogenesis. *Antioxidants* **2022**, *11*(2), DOI: 10.3390/antiox11020358.
(27) Thangavelu, L.; Altamimi, A.; Ghaboura, N.; Babu, M. A.; Roopashree, R.; Sharma, P.; Pal, P.;

Choudhary, C.; Prasad, G.; Sinha, A.; et al. Targeting the p53-p21 axis in liver cancer: linking cellular senescence to tumor suppression and progression. *Pathol. Res. Pract.* **2024**, *263*, 155652, DOI: 10.1016/j.prp.2024.155652.

(28) Mishima, M.; Takai, A.; Takeda, H.; Iguchi, E.; Nakano, S.; Fujii, Y.; Ueno, M.; Ito, T.; Teramura, M.; Eso, Y.; et al. Tert upregulation promotes cell proliferation via degradation of p21 and increases carcinogenic potential. *J. Pathol.* **2024**, *264*(3), 318-331, DOI: 10.1002/path.6351.

(29) Cai, X.; Gao, J.; Yan, Z.; Zhang, H.; Guo, D.; Zhang, S. March5 promotes hepatocellular carcinoma progression by inducing p53 ubiquitination degradation. *J. Cancer. Res. Clin. Oncol.* **2024**, *150*(6), 303, DOI: 10.1007/s00432-024-05782-7.

(30) Liu, Y.; Su, Z.; Tavana, O.; Gu, W. Understanding the complexity of p53 in a new era of tumor suppression. *Cancer Cell* **2024**, *42*(6), 946-967, DOI: 10.1016/j.ccell.2024.04.009.

(31) Lai, L.; Tan, M.; Hu, M.; Yue, X.; Tao, L.; Zhai, Y.; Li, Y. Important molecular mechanisms in ferroptosis. *Mol. Cell. Biochem.* **2024**, DOI: 10.1007/s11010-024-05009-w.

(32) Song, B.; Yang, P.; Zhang, S. Cell fate regulation governed by p53: friends or reversible foes in cancer therapy. *Cancer Commun.* **2024**, *44*(3), 297-360, DOI: 10.1002/cac2.12520.

(33) Mao, C.; Lei, G.; Zhuang, L.; Gan, B. Phospholipase ipla2 β acts as a guardian against ferroptosis. *Cancer Commun.* **2021**, *41*(11), 1082-1085, DOI: 10.1002/cac2.12231.

Footnotes:

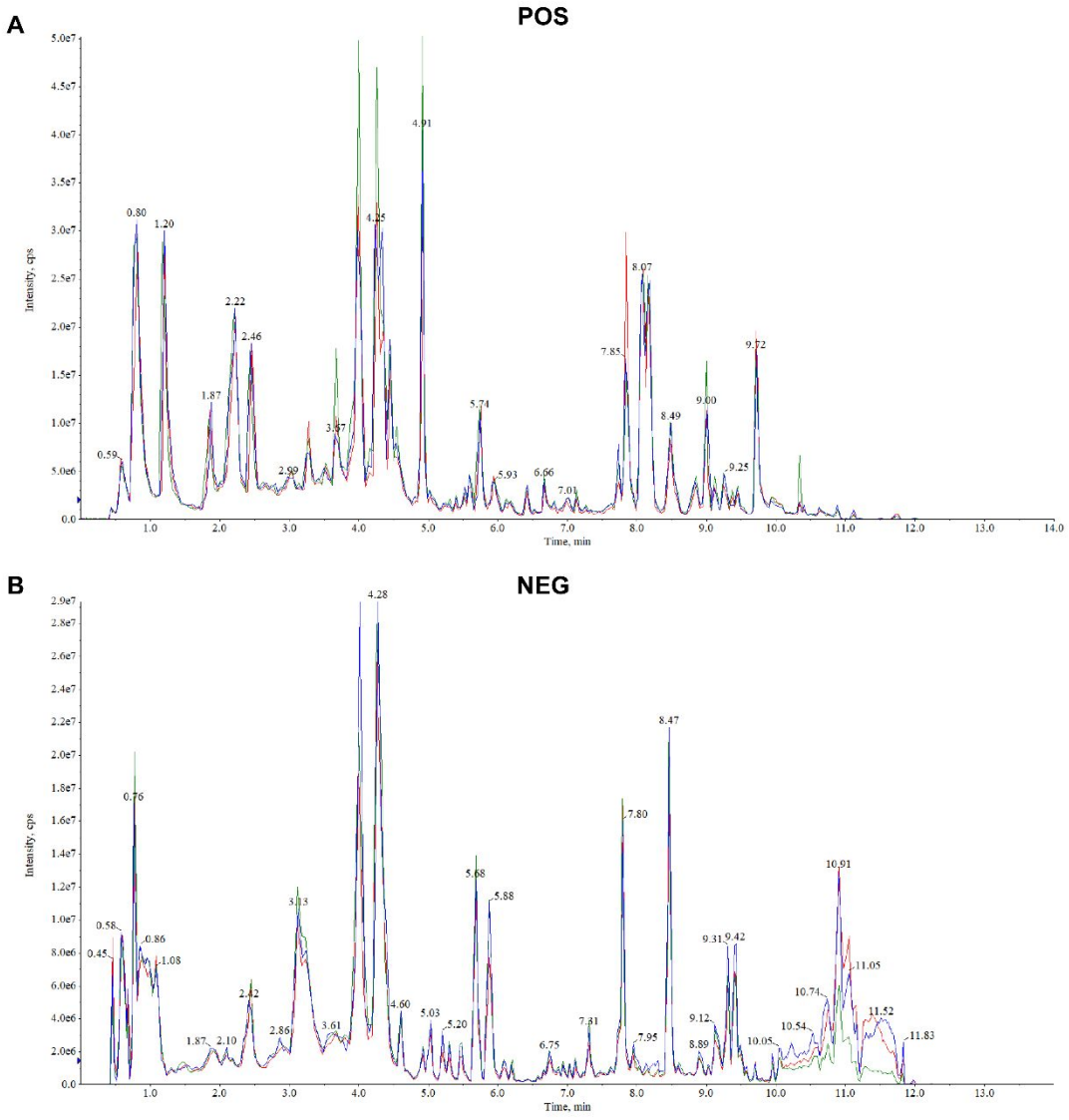

Fig. 1: The Therapeutic Component in JDS.

(A) TIC plot of JDS in positive ion mode; (B) TIC plot of JDS in negative ion mode.

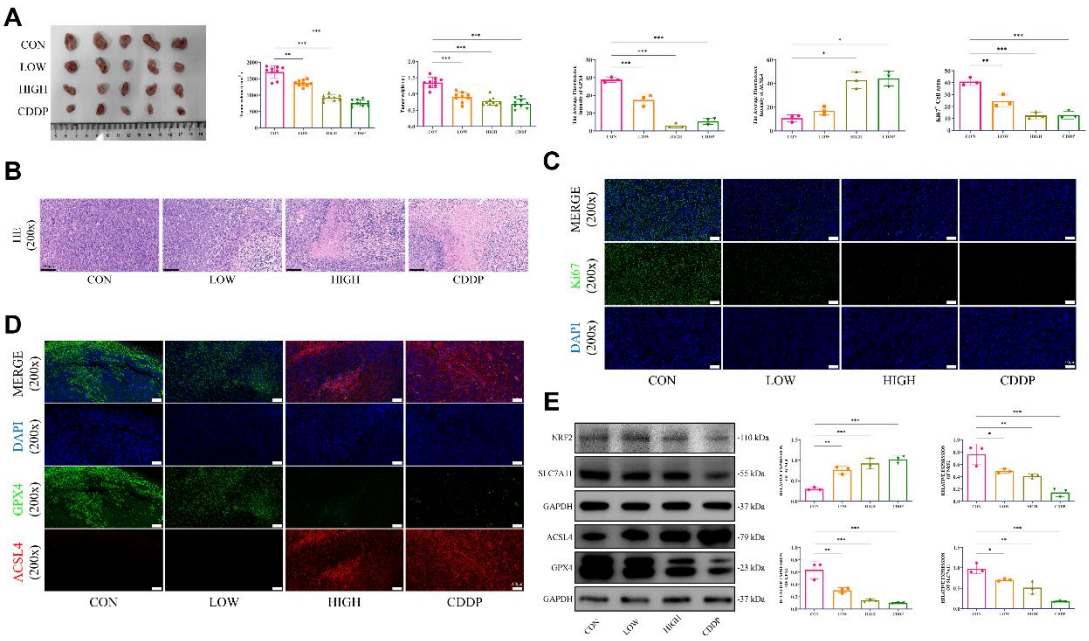

Fig. 2: JDS inhibits xenograft tumour growth in vivo.

(A) Representative images of transplanted tumours and quantitative results of body weight and volume; (B) Representative images of HE staining of transplanted tumours; (C) Representative images and quantitative results of Ki67 immunofluorescence in transplanted tumours; (D) Representative images and quantitative results of GPX4 and ASCL4 immunofluorescence in transplanted tumours; (E) Representative images and quantitative results of WB assay for iron-death-related proteins. (E) Representative images and quantification results of Ferroptosis-related proteins detected by WB. *Mean ± standard deviation (Mean ± SD, n=3) was used for statistical plots. *P < 0.05, ***P < 0.01,***P < 0.001 vs con group.*

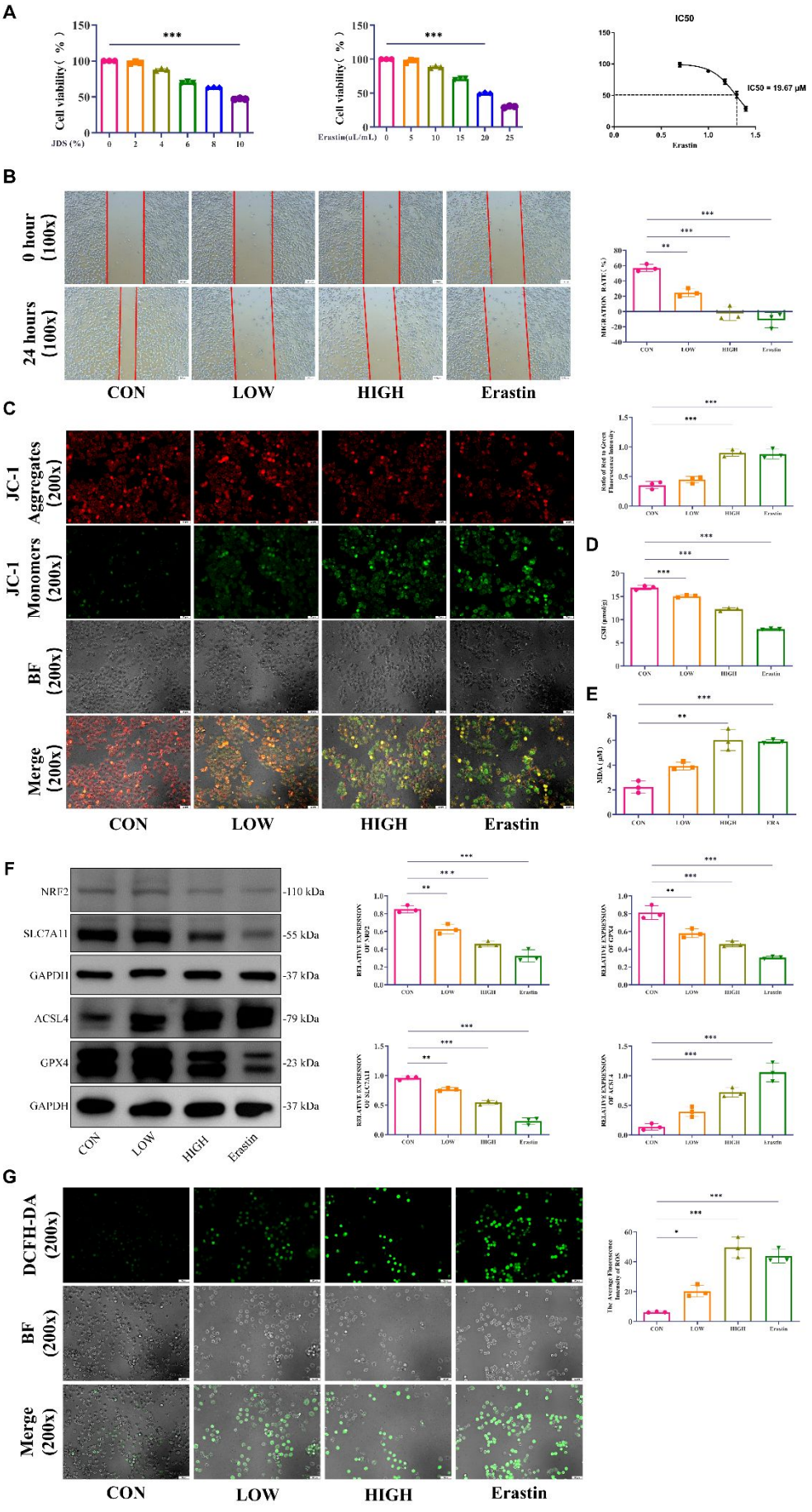
A
Cell viability(%)
JDS (%)
Erastin(uL/mL)
IC50
IC50 = 19.67 μM
Erastin
B
0 hour (100x)
24 hours (100x)
CON
LOW
HIGH
Erastin
MIGRATION RATE(%)
C
JC-1 Aggregates (200x)
JC-1 Monomers (200x)
BF (200x)
Merge (200x)
D
CSH (pmol/g)
E
MDA (μM)
F
NRF2
SLC7A11
GAPDH
ACSL4
GPX4
-110 kDa
-55 kDa
-37 kDa
-79 kDa
-23 kDa
RELATIVE EXPRESSION OF NRF2
RELATIVE EXPRESSION OF GPX4
RELATIVE EXPRESSION OF SLC7A11
RELATIVE EXPRESSION OF ACSL4
G
DCFH-DA (200x)
BF (200x)
Merge (200x)

Fig. 3: JDS promotes GPX4-mediated Ferroptosis process to inhibit HepG2 cell proliferation.

(A) Survival rate and IC50 values of HepG2 cells after 24 h of JDS and Erastin intervention; (B) representative images and quantification results of migration rate in scratch assay; (C) representative images and quantification results of mitochondrial membrane potential; (D) quantification results of GSH; (E) quantification results of MDA; (F) representative images and quantification results of iron-death-related proteins in WB assay; (G) representative images and quantification results of ROS; (H) representative images and quantification results of ROS. results; (G) Representative images and quantification results of ROS; *Mean ± standard deviation (Mean ± SD, n=3) was used for statistical plots. *P < 0.05, ***P < 0.01,***P < 0.001 vs con group.*

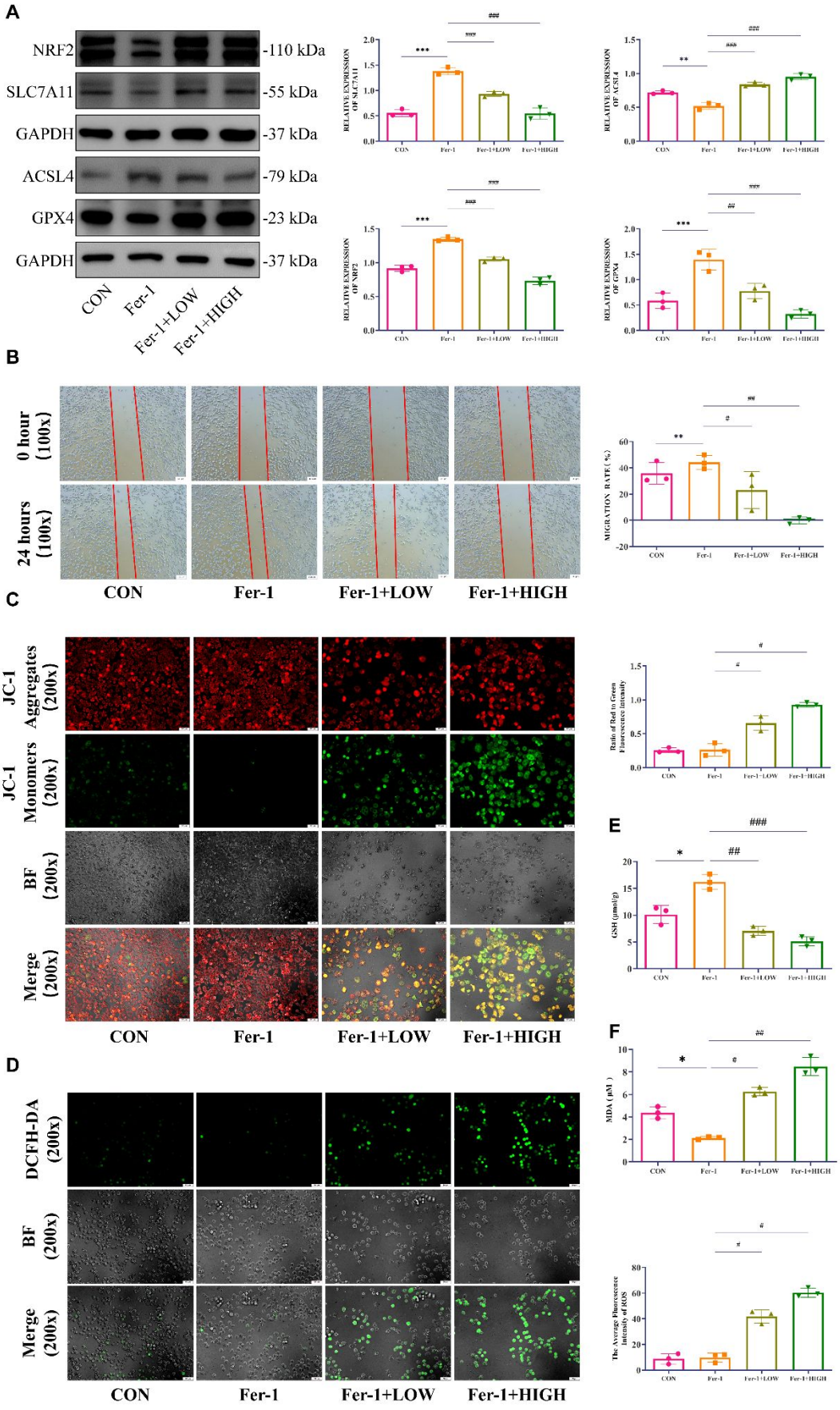
A
NRF2
SLC7A11
GAPDH
ACSL4
GPX4
GAPDH
-110 kDa
-55 kDa
-37 kDa
-79 kDa
-23 kDa
-37 kDa
CON
Fer-1
Fer-1+LOW
Fer-1+HIGH
RELATIVE EXPRESSION OF SLC7A11
RELATIVE EXPRESSION OF ACSL4
RELATIVE EXPRESSION OF NRF2
RELATIVE EXPRESSION OF GPX4
B
0 hour (100x)
24 hours (100x)
MIGRATION RATE (%)
C
JC-1 Aggregates (200x)
JC-1 Monomers (200x)
BF (200x)
Merge (200x)
Ratio of Red to Green Fluorescence Intensity
D
DCFH-DA (200x)
BF (200x)
Merge (200x)
The Average Fluorescence Intensity of ROS
E
GSH (μmol/g)
F
MDA (μM)

596

Fig. 4: JDS promotes Ferroptosis reversal of the protective effect of Fer-1 in HepG2 cells.

(A) Representative images and quantification results of Ferroptosis-related proteins detected by WB; (B) Representative images and quantification results of mobility shift in scratch assay; (C) Representative images and quantification results of mitochondrial membrane potential; (D) Representative images and quantification results of ROS; (E) Quantification results of GSH; (F) Quantification results of MDA. *Mean ± standard deviation (Mean ± SD, n=3) was used for statistical plots. *P < 0.05, ***P < 0.001 vs con group; ##P < 0.01, ###P < 0.001 vs Fer-1 group*

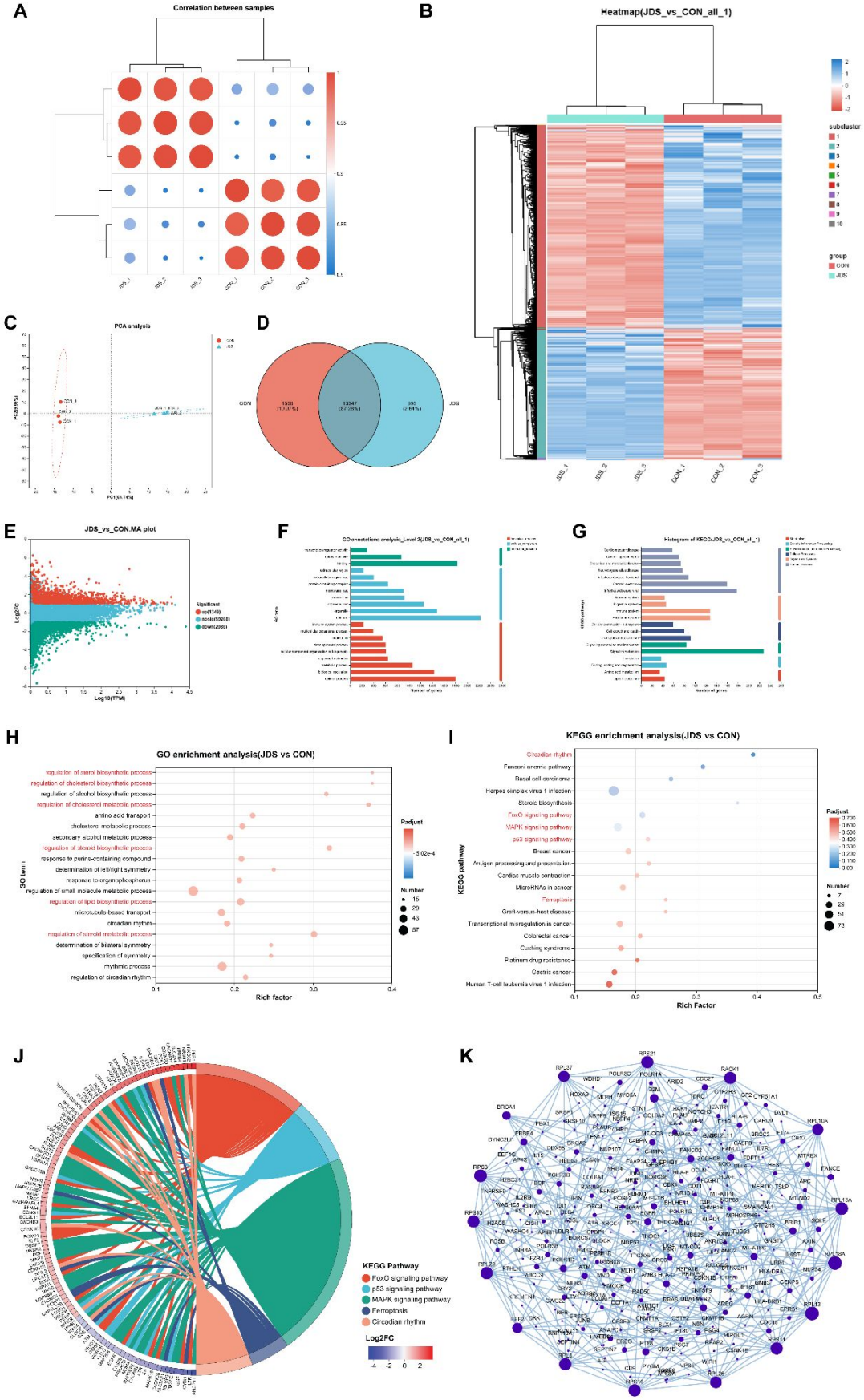
A
Correlation between samples
B
Heatmap(JDS_vs_CON_all_1)
subcluster
group
CON
JDS
C
PCA analysis
D
CON
JDS
E
JDS_vs_CON.MA plot
Significant
F
G
H
GO enrichment analysis(JDS vs CON)
GO term
Rich factor
Padjust
Number
I
KEGG enrichment analysis(JDS vs CON)
KEGG pathway
Rich Factor
J
KEGG Pathway
FoxO signaling pathway
p53 signaling pathway
MAPK signaling pathway
Ferroptosis
Circadian rhythm
Log2FC
K

604

Fig. 5: Transcriptomic analyses targeting the interventional effects of JDS on HepG2 cells.

(A) Heatmap of inter-sample correlation; (B) PCA downscaling distribution plot; (C) Venn diagram of sample gene differences between two groups; (D) Heatmap of differential gene clustering analysis between two groups; (E) Scatter plot of differential gene volcano between two groups; (F) Differential gene GO annotation analysis between two groups; (G) Differential gene KEGG annotation analysis between two groups; (H) Differential gene GO enrichment analysis between two groups; (I) differential gene KEGG enrichment analysis between two groups; (J) chordal plot of differential gene GO enrichment analysis between two groups; (K) protein interaction network analysis plot.

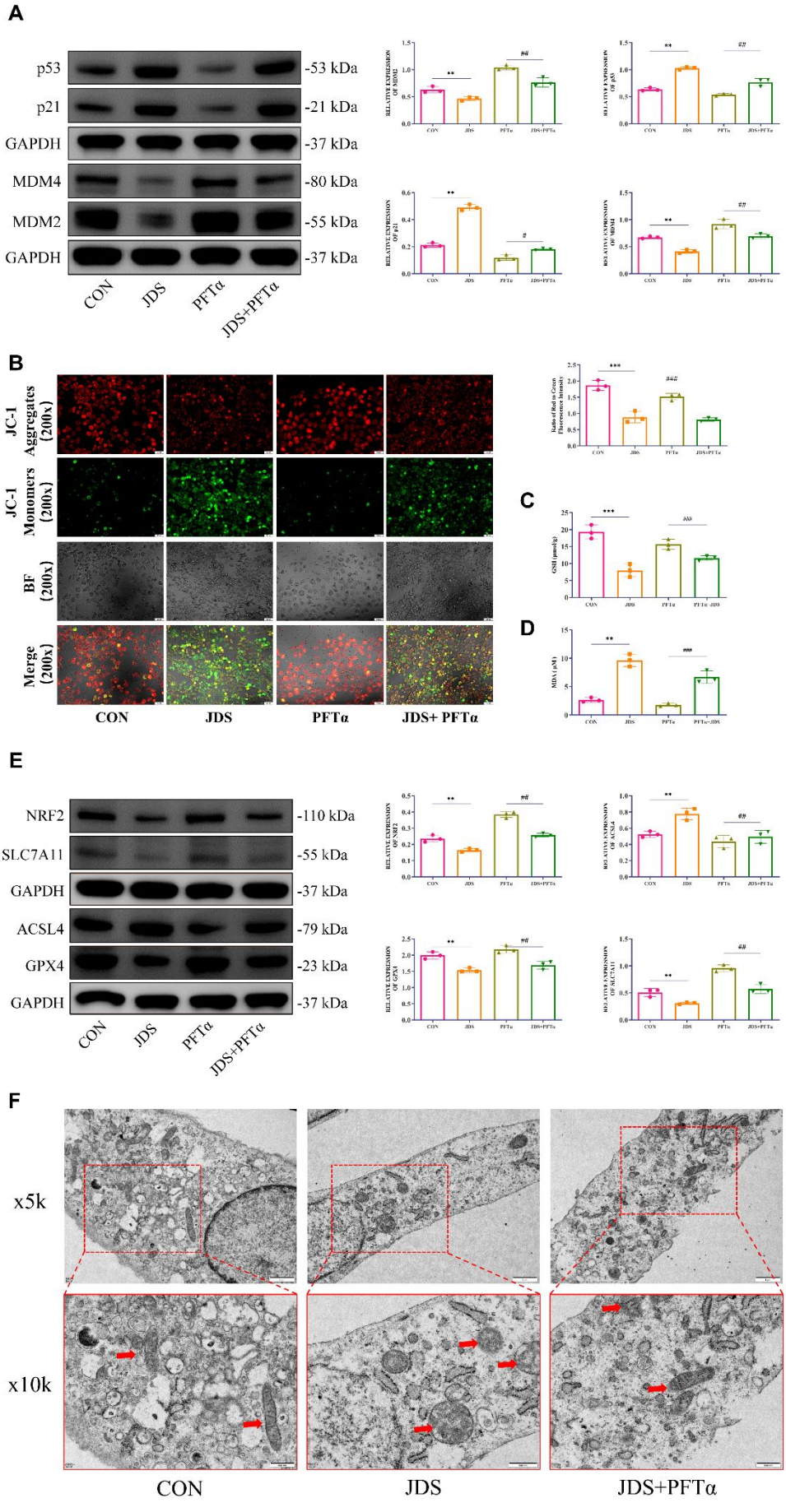
A
p53
p21
GAPDH
MDM4
MDM2
GAPDH
-53 kDa
-21 kDa
-37 kDa
-80 kDa
-55 kDa
-37 kDa
CON
JDS
PFTα
JDS+PFTα
B
JC-1 Aggregates (200x)
JC-1 Monomers (200x)
BF (200x)
Merge (200x)
CON
JDS
PFTα
JDS+ PFTα
C
D
E
NRF2
SLC7A11
GAPDH
ACSL4
GPX4
GAPDH
-110 kDa
-55 kDa
-37 kDa
-79 kDa
-23 kDa
-37 kDa
F
x5k
x10k
CON
JDS
JDS+PFTα

Fig. 6: JDS promotes Ferroptosis by activating the p53 signaling pathway.

(A) Representative images and quantification results of p53 signaling pathway proteins detected by WB; (B) Representative images and quantification results of mitochondrial membrane potential; (C) Quantification results of GSH; (D) Quantification results of MDA; (E) Representative images and quantification results of iron-death-associated proteins detected by WB; (F) Transmission electron microscopy to observe the changes in the morphology of mitochondria in the cells of each group. *Mean ± standard deviation (Mean ± SD, n=3) was used for statistical plots. *P < 0.05, **P < 0.01,***P < 0.001 vs con group; #P < 0.05,##P < 0.01, ###P < 0.001 vs JDS group*

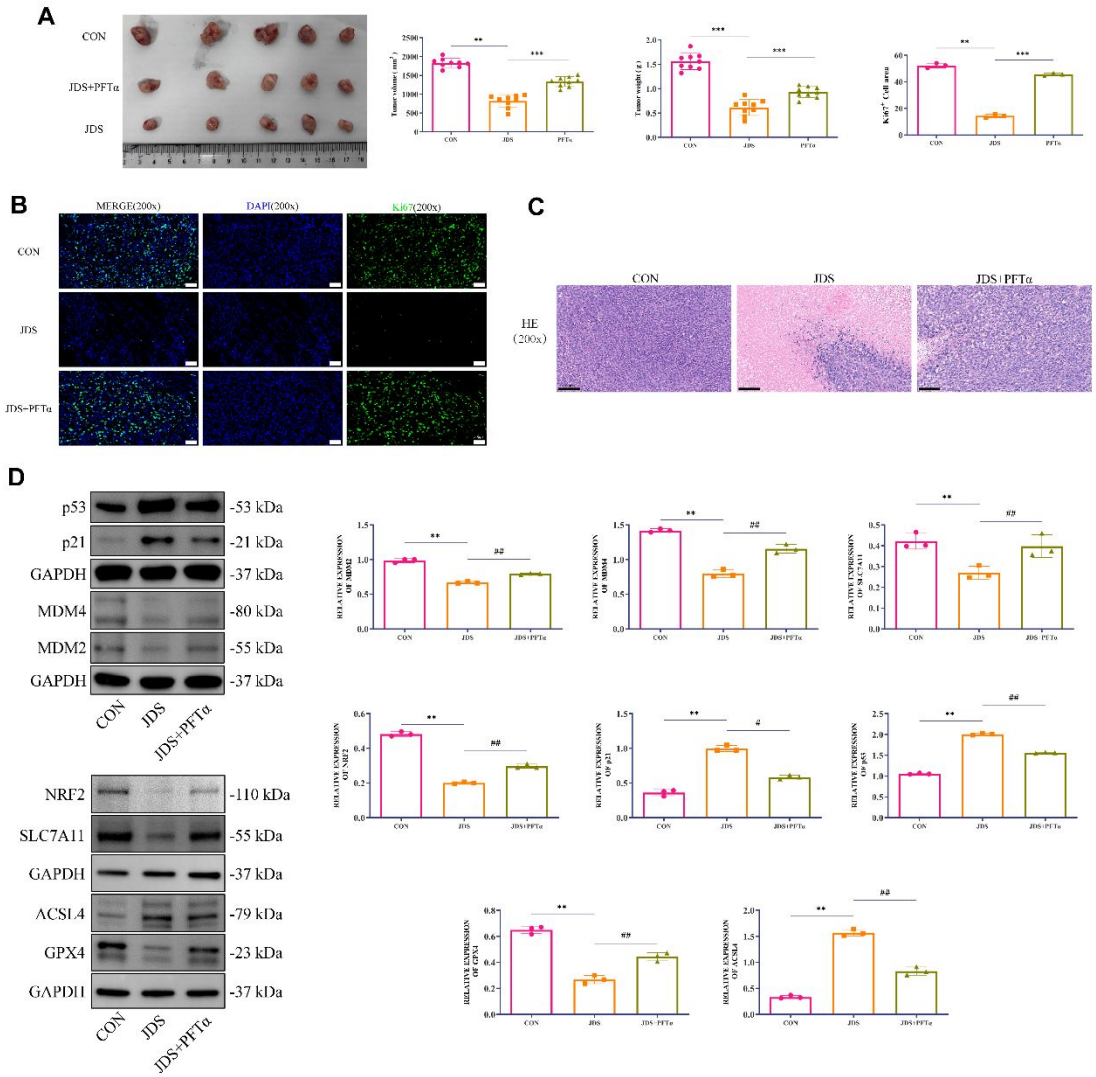

Fig. 7: PFT-α intervention attenuates the effect of JDS on xenograft tumour Ferroptosis.

(A) Representative images of transplanted tumours and quantitative results of weight and volume; (B) Representative images and quantitative results of Ki67 immunofluorescence in transplanted tumours; (C) Representative images of HE staining of transplanted tumours; (D) Representative images and quantitative results of WB detection of the p53 signaling pathway and iron-death-related proteins. *Mean ± standard deviation (Mean ± SD, n=3) was used for statistical plots. *P < 0.05, **P < 0.01,***P < 0.001 vs con group; #P < 0.05,##P < 0.01, ###P < 0.001 vs JDS group*

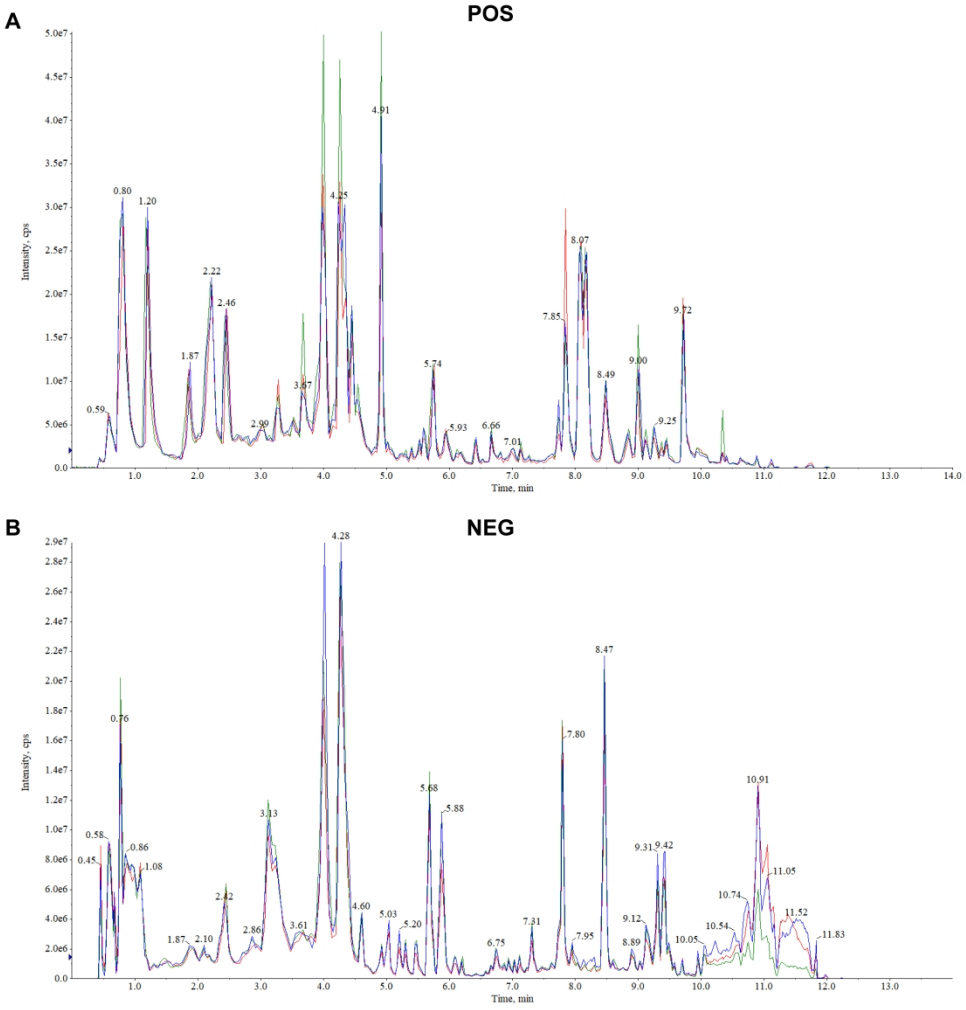

Figure1

381x396mm (300 x 300 DPI)

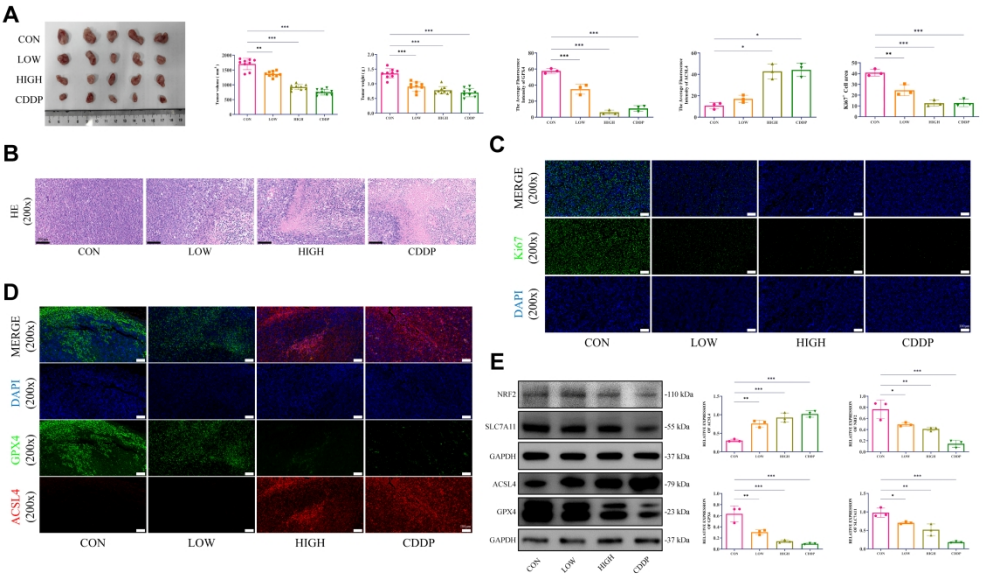

Figure2

371x218mm (300 x 300 DPI)

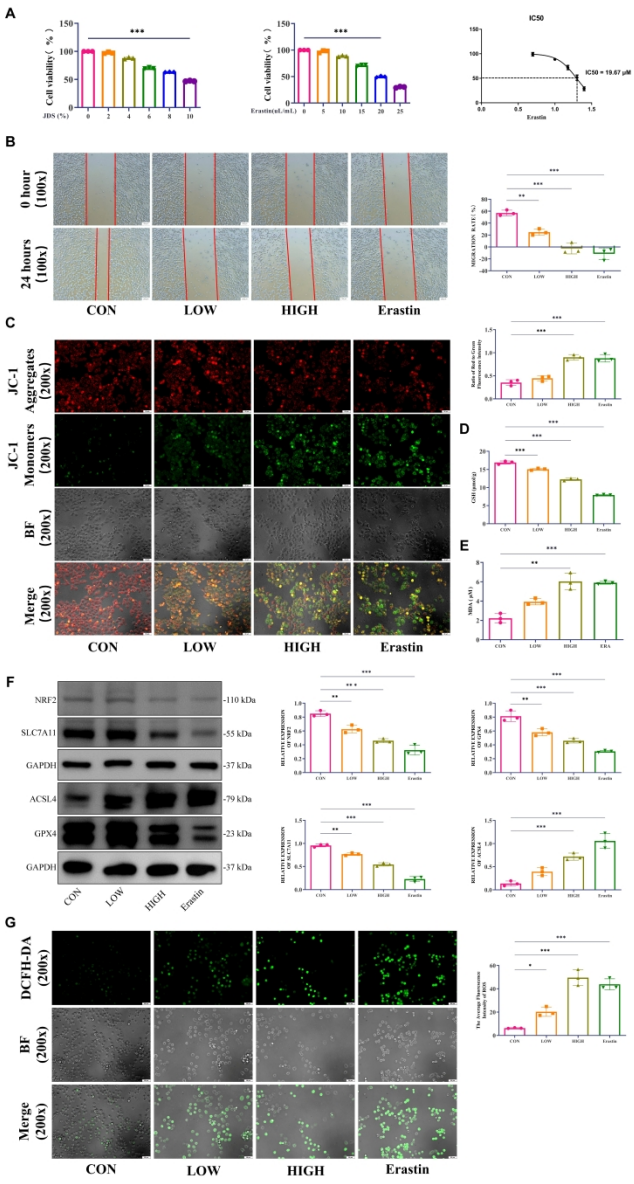

Figure3

381x699mm (300 x 300 DPI)

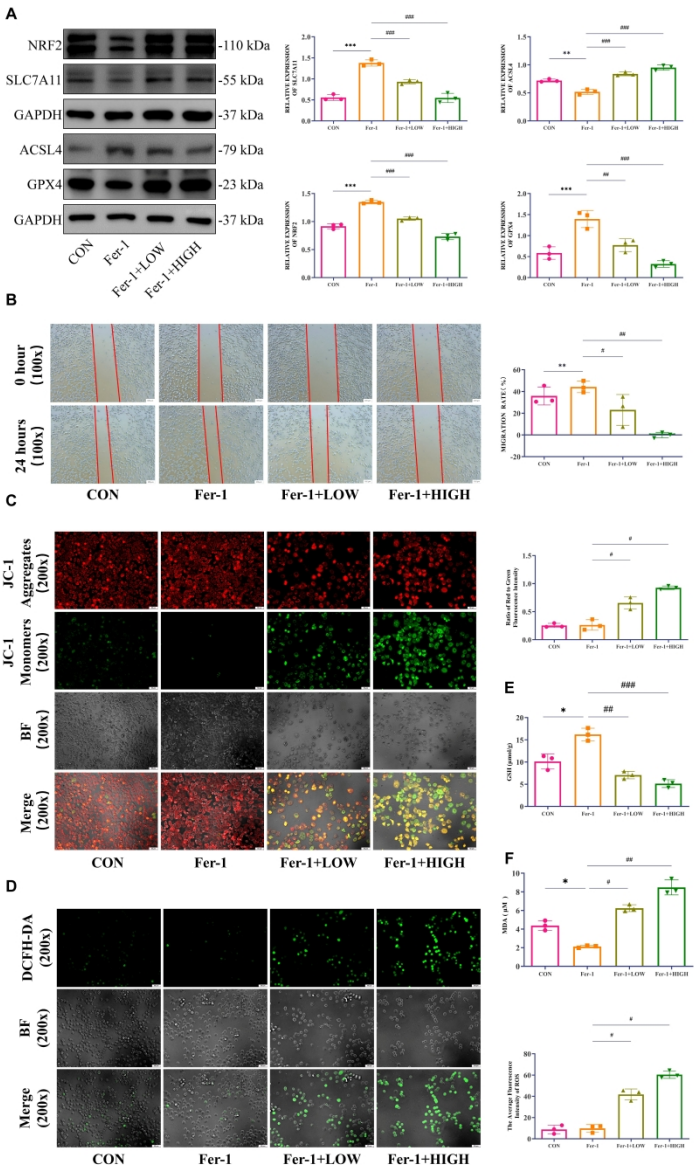

Figure4

386x633mm (300 x 300 DPI)

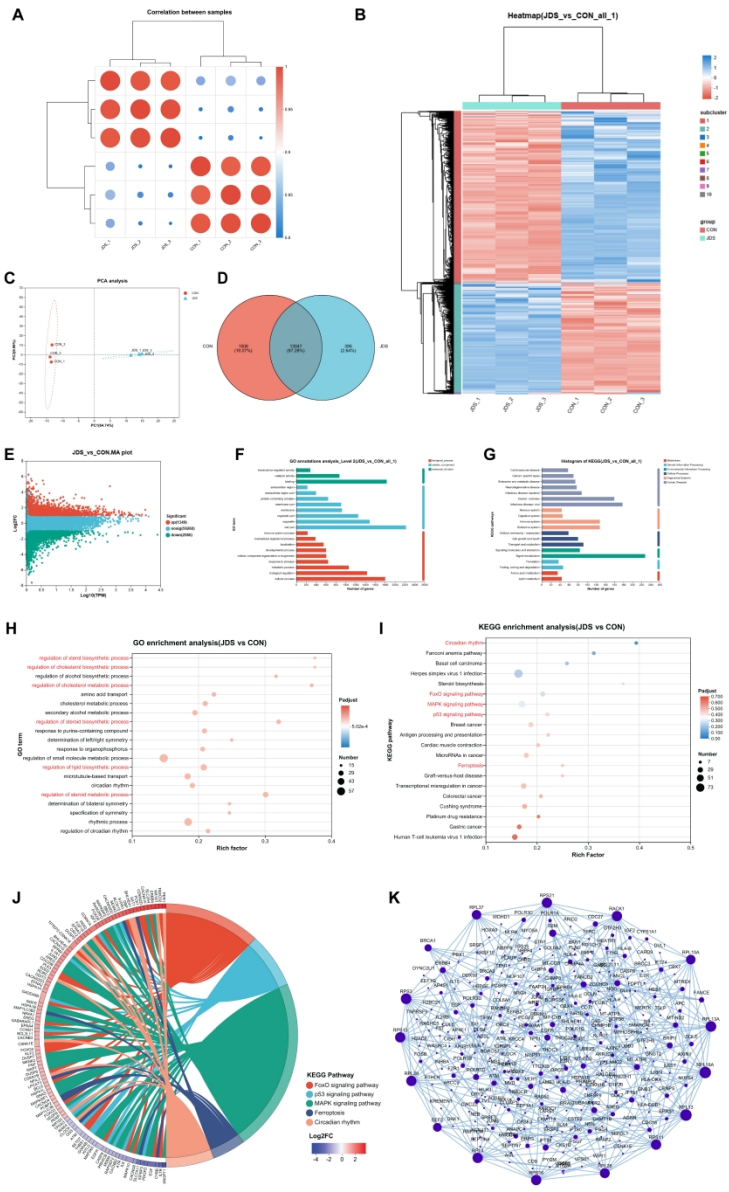

Figure5

386x618mm (300 x 300 DPI)

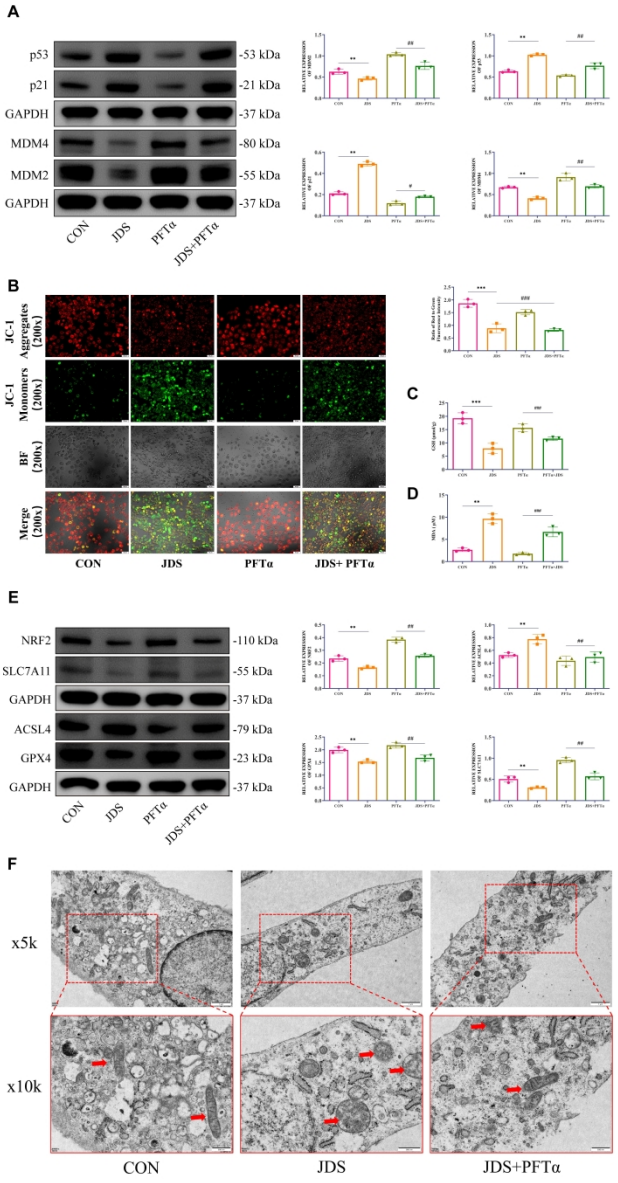

Figure6

335x609mm (300 x 300 DPI)

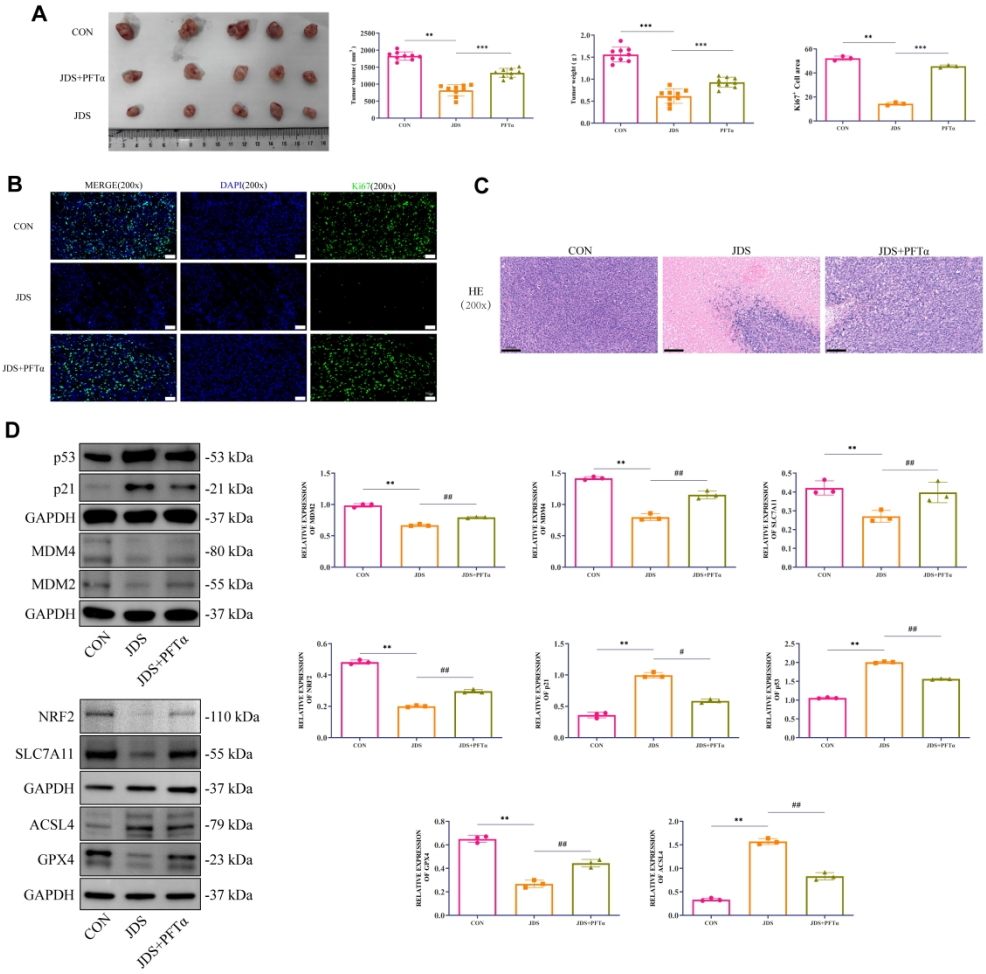

Figure7

381x379mm (300 x 300 DPI)

original western blot for three repeats-Figure2

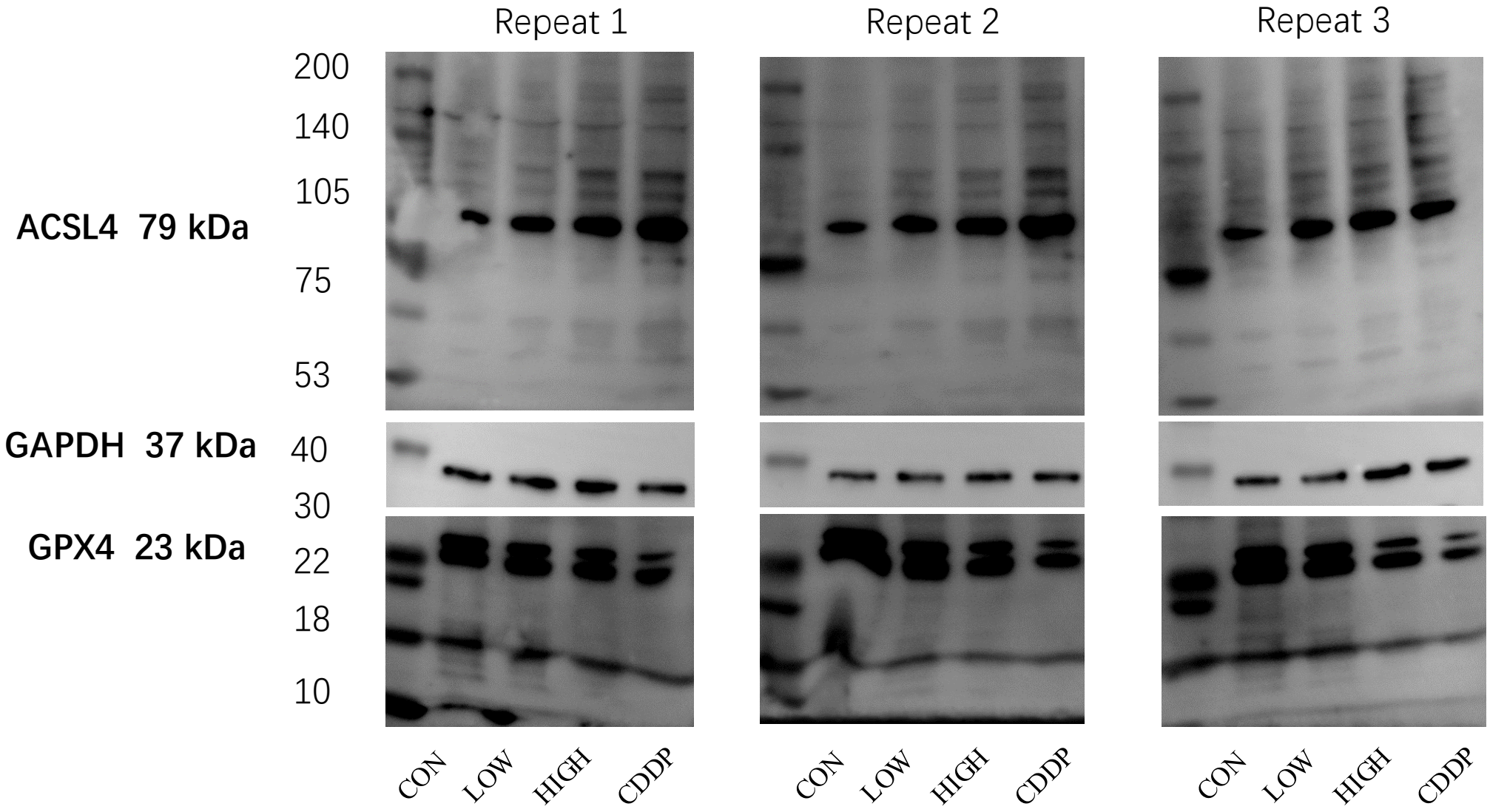

original western blot for three repeats-Figure2

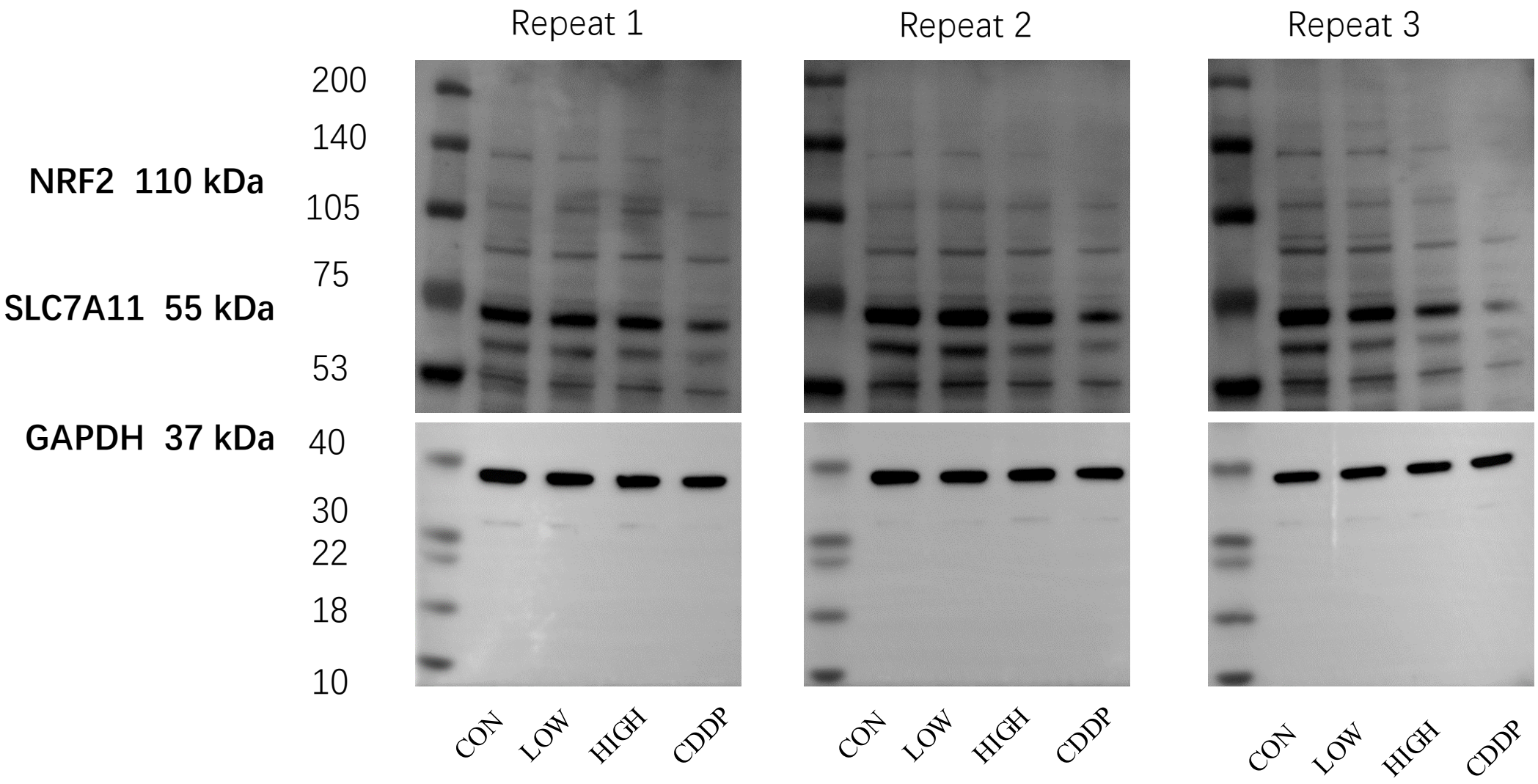

original western blot for three repeats-Figure3

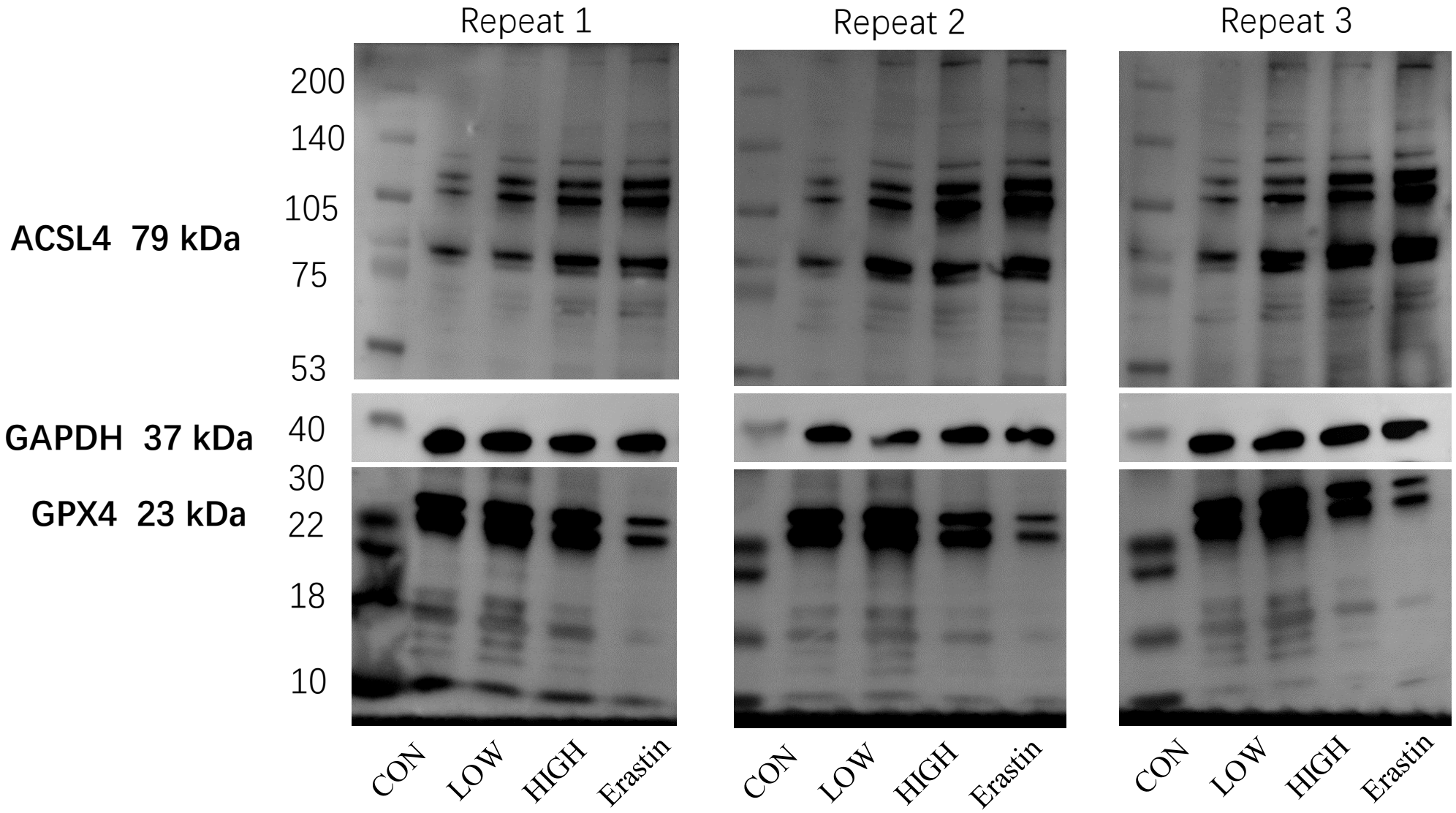

original western blot for three repeats-Figure3

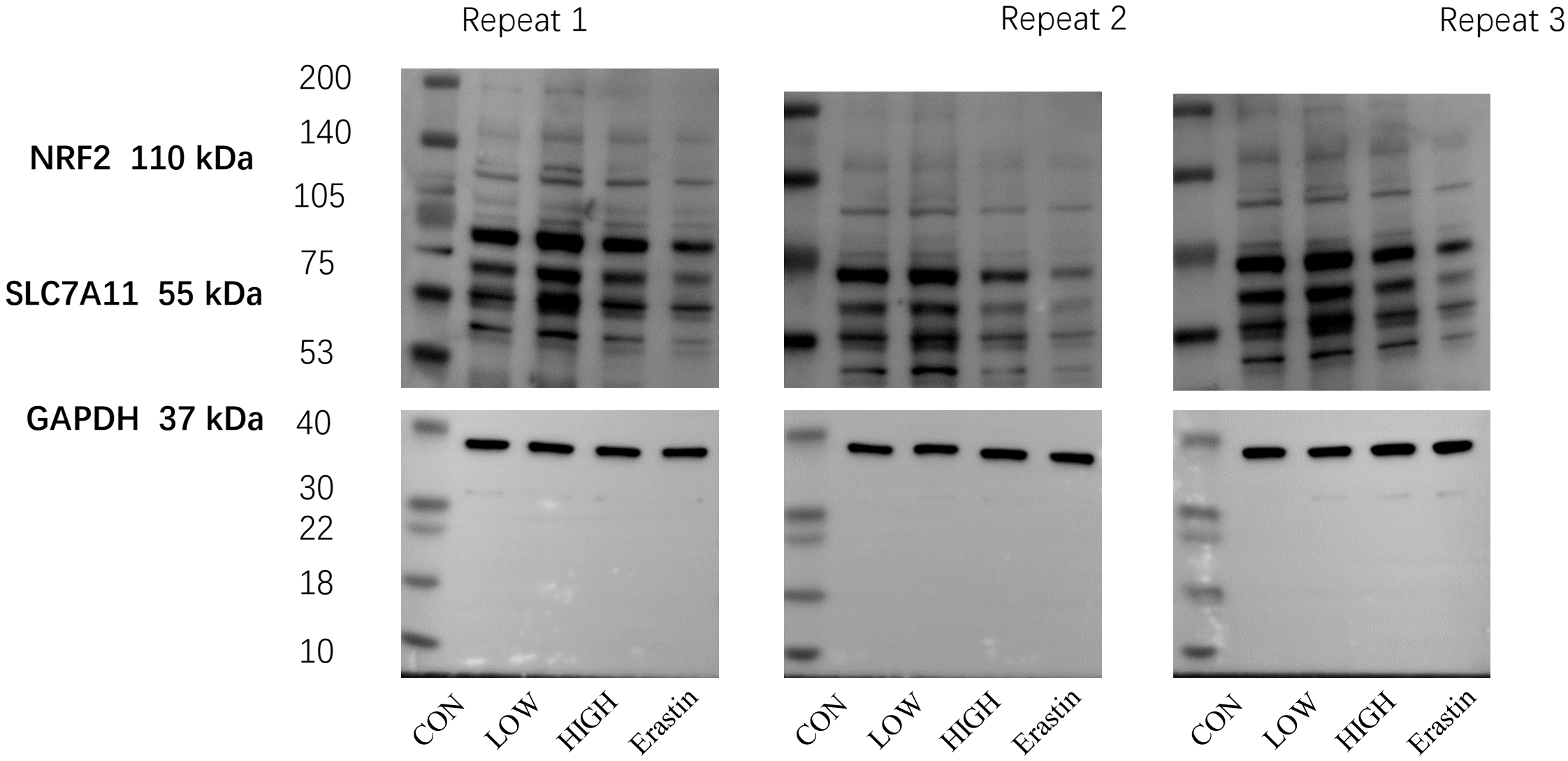

original western blot for three repeats-Figure4

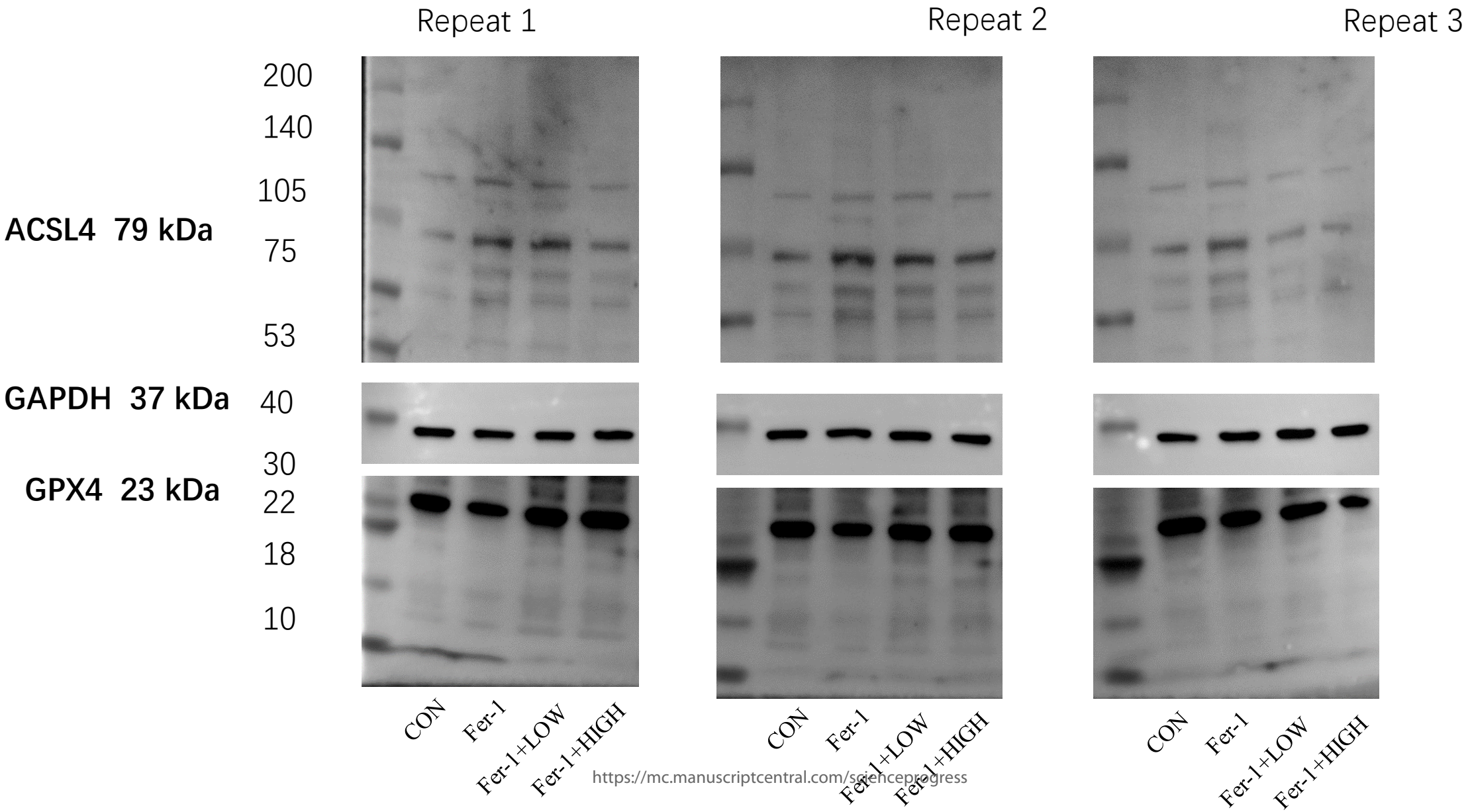

original western blot for three repeats-Figure4

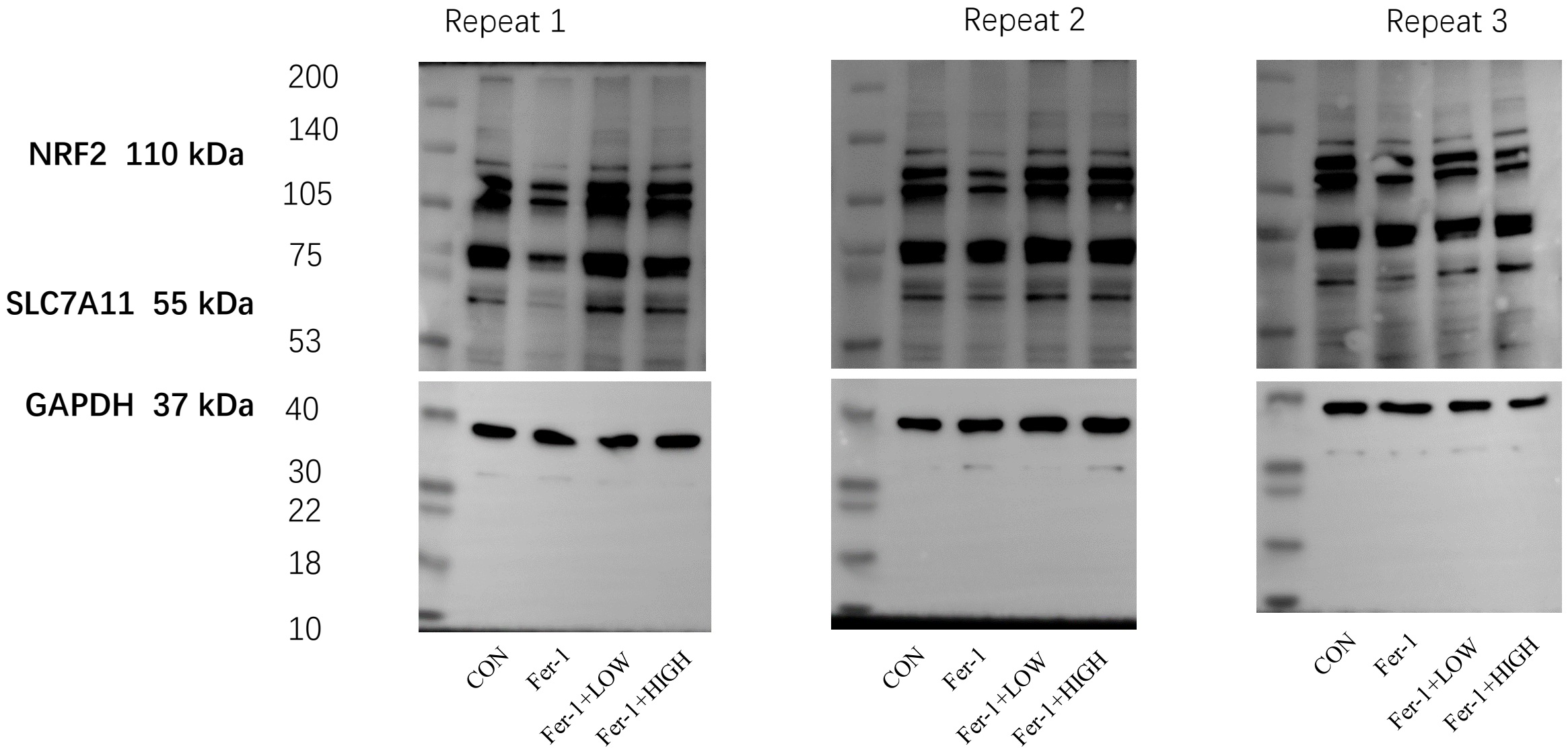

original western blot for three repeats-Figure6

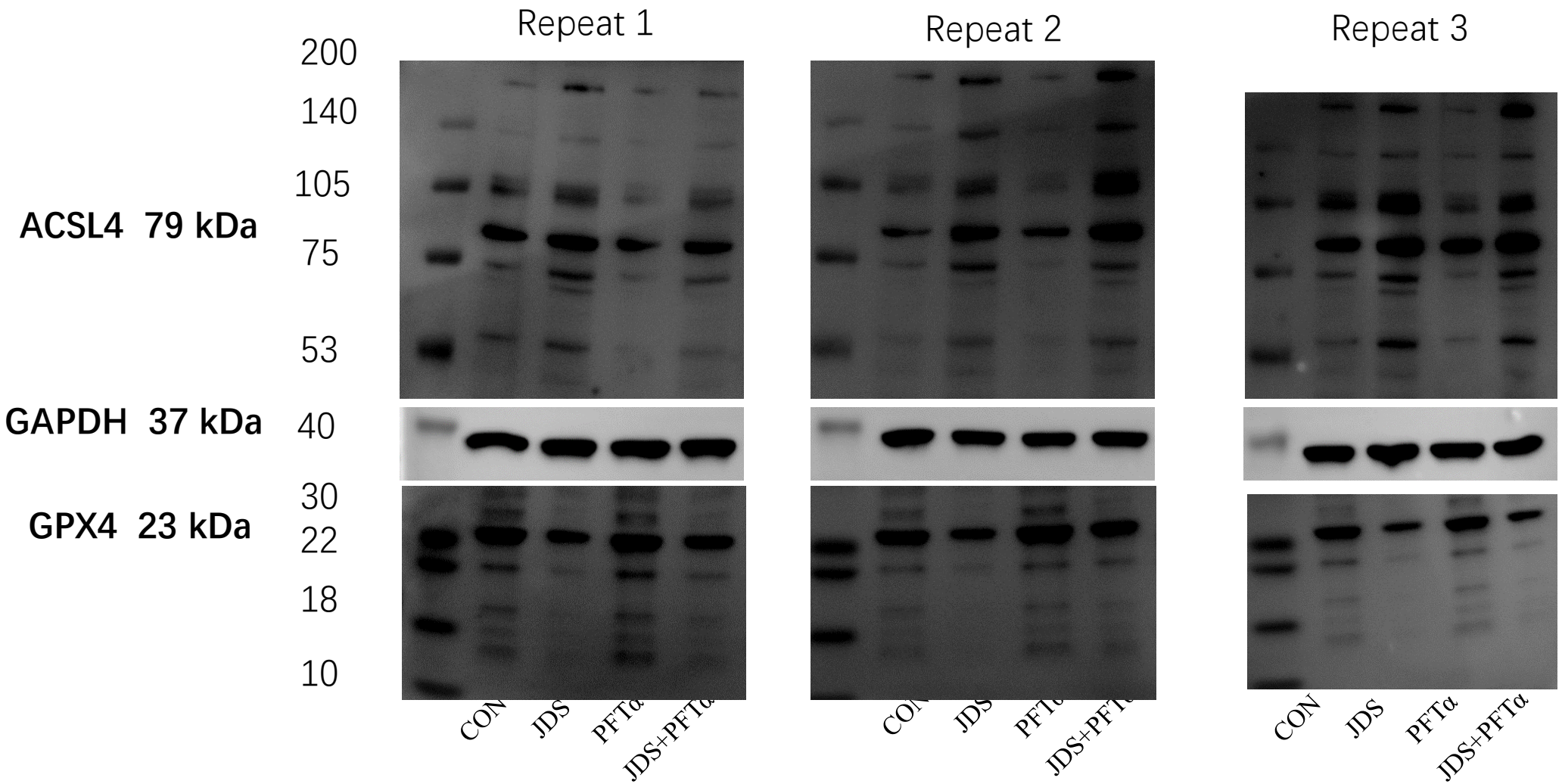

original western blot for three repeats-Figure6

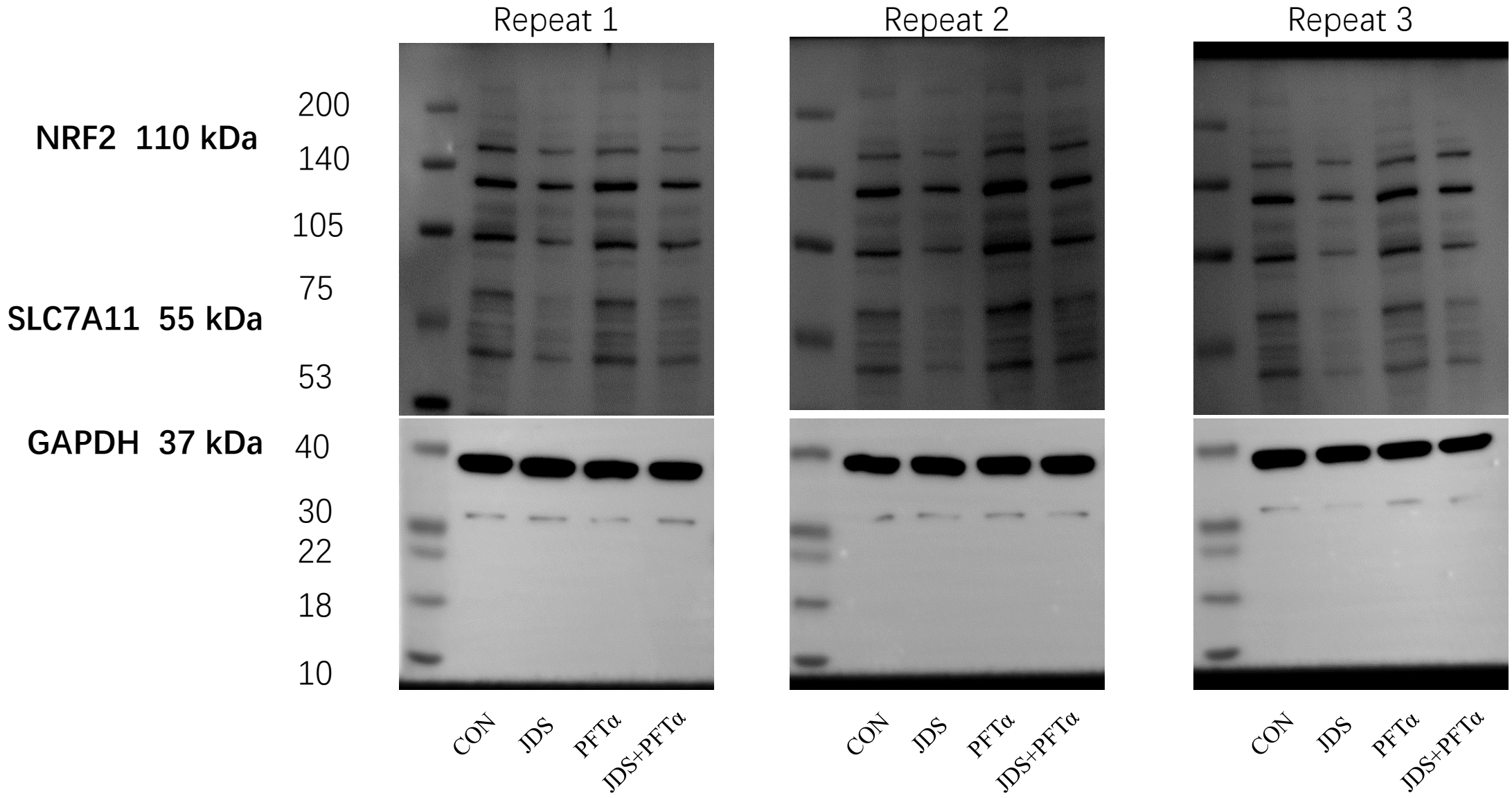

original western blot for three repeats-Figure6

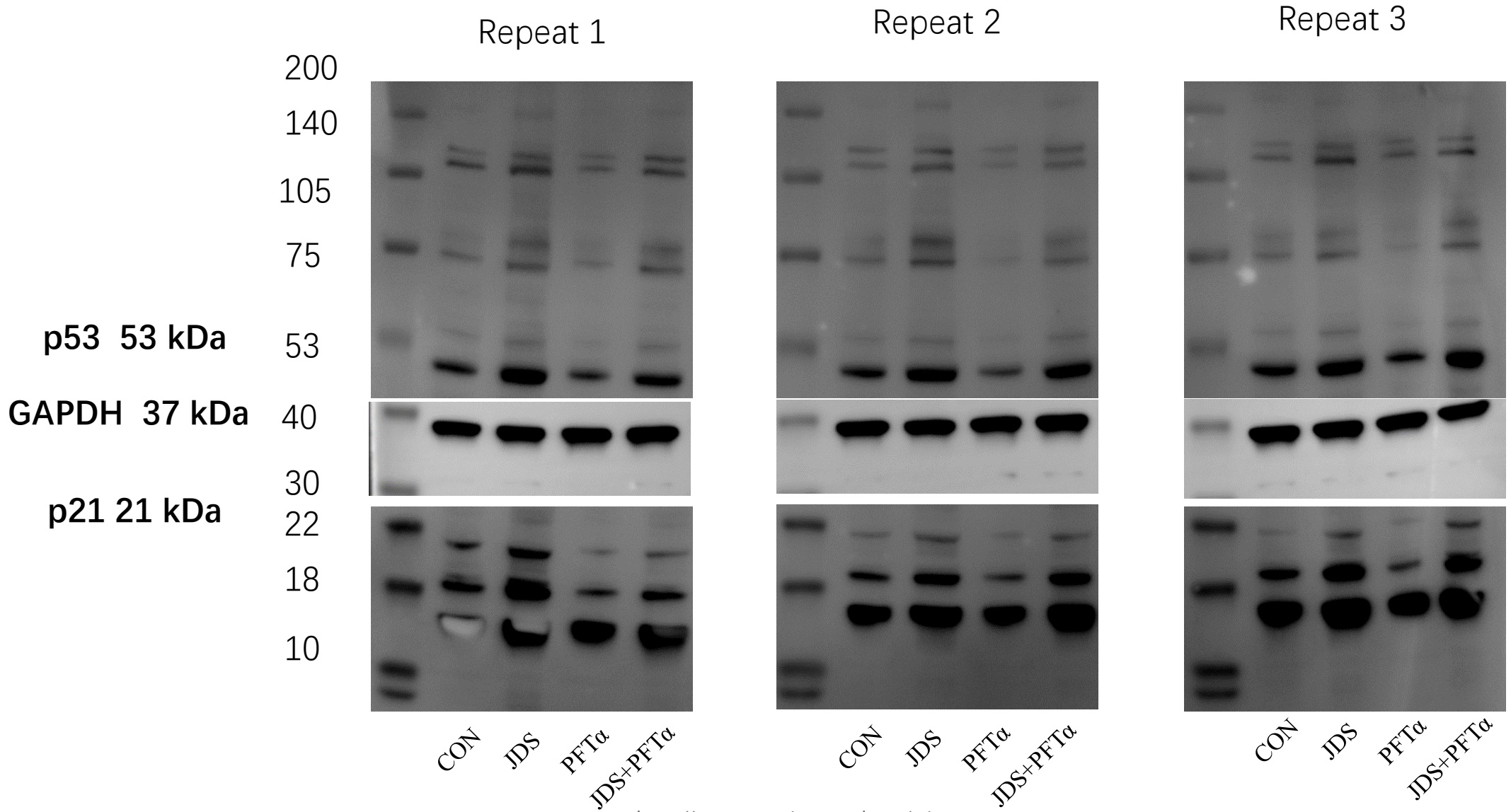

original western blot for three repeats-Figure6

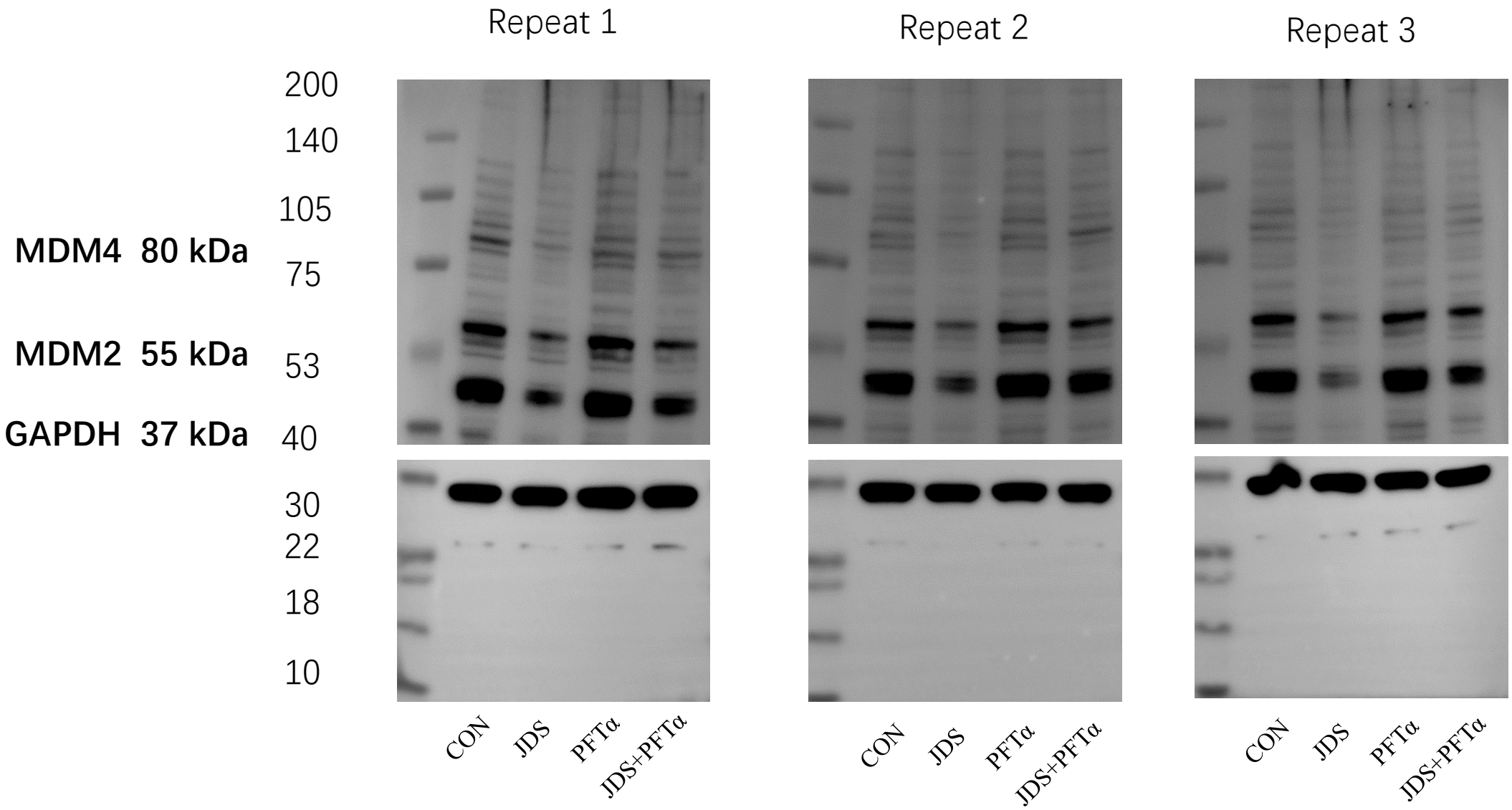

original western blot for three repeats-Figure7

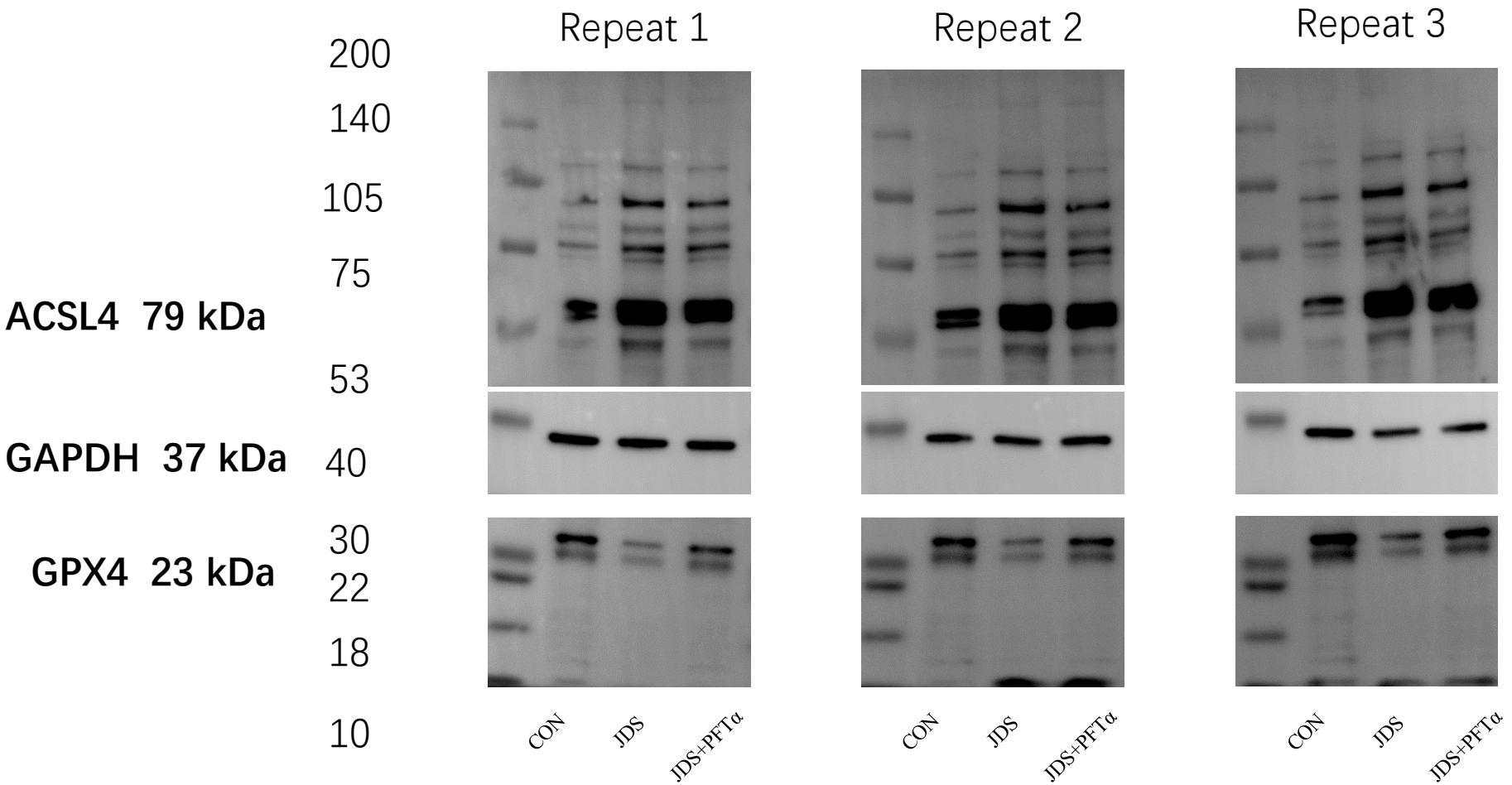

original western blot for three repeats-Figure7

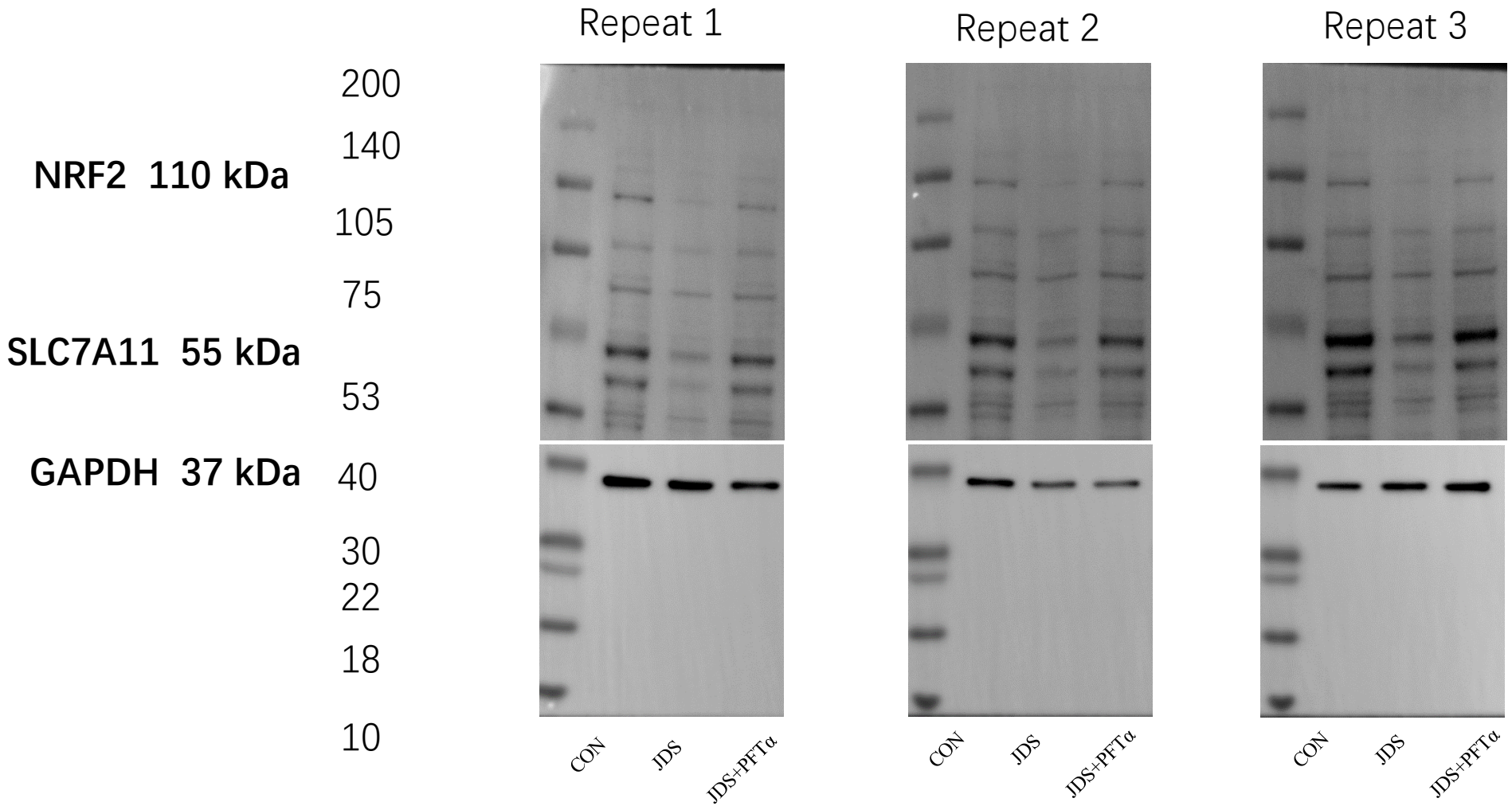

original western blot for three repeats-Figure7

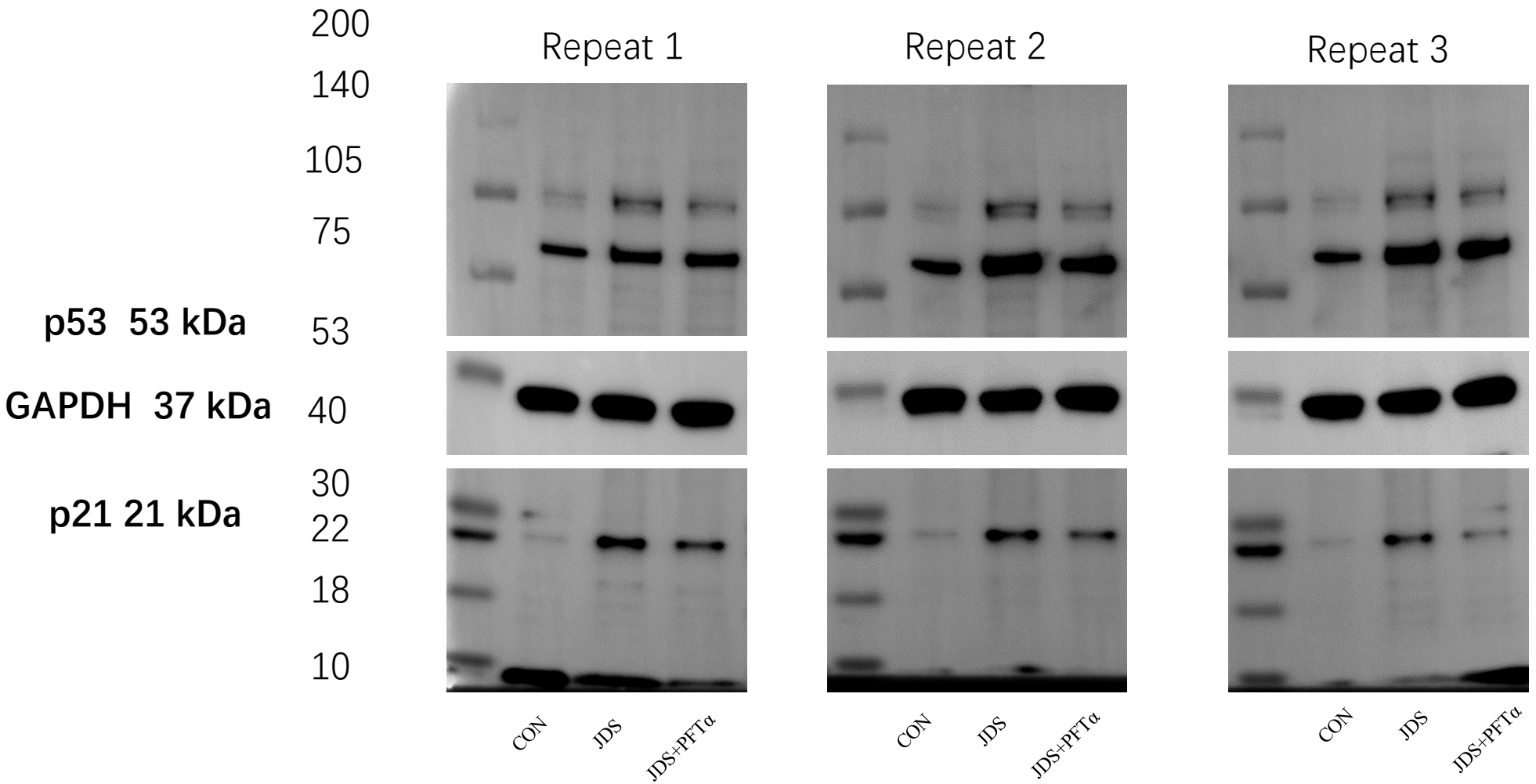

original western blot for three repeats-Figure7

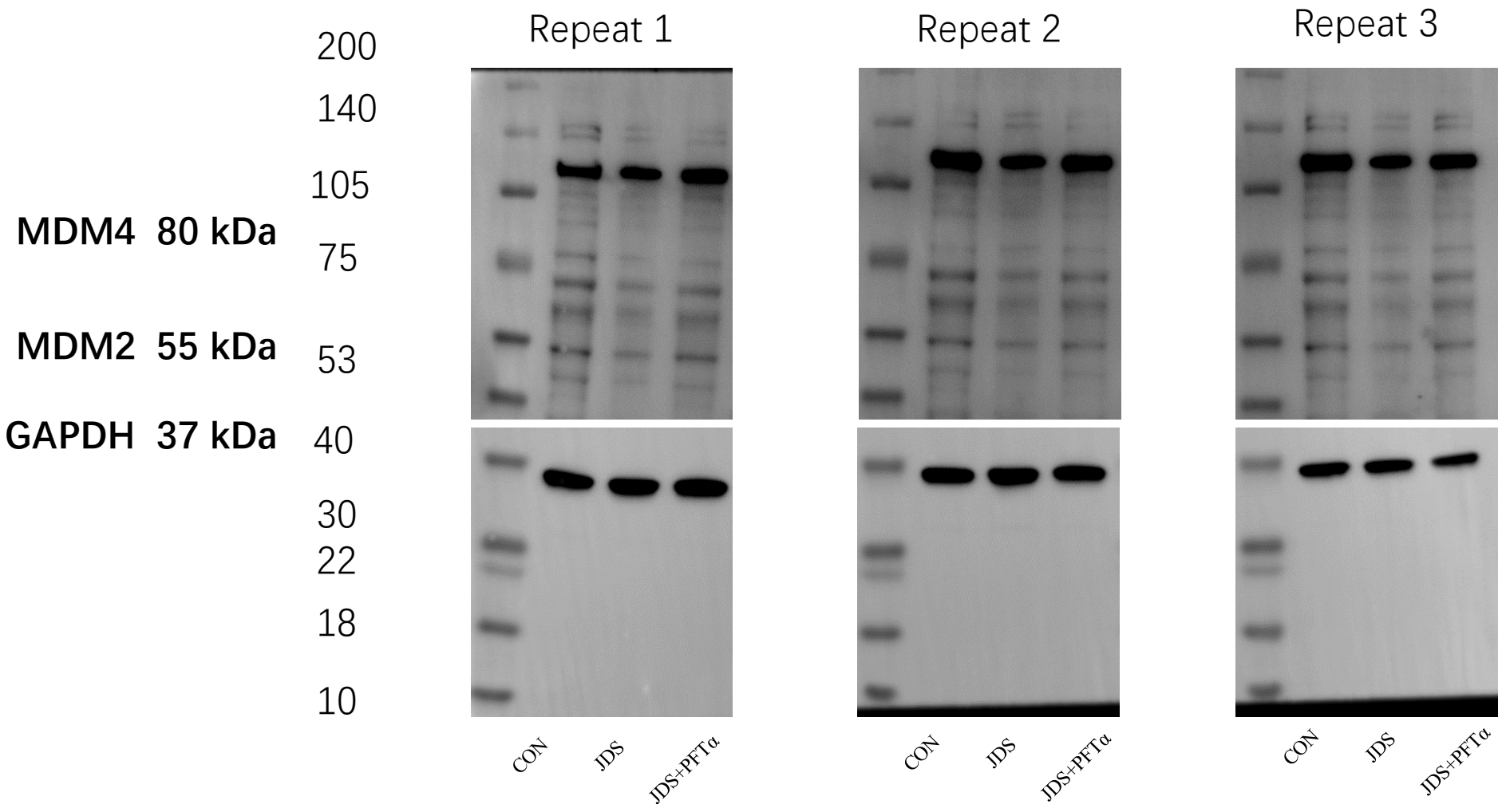

Compounds	Class I	Class II	Formula	Q1 (Da)	Q3 (Da)	Molecular weight (Da)	Ionization model	JDS1	JDS2	JDS3
5-Methoxyfurfural*	Others	Aldehyde compounds	C6H6O3	127.04	53.04	126.0317	[M+H]+	36267595	35299932	35160594
Diosmetin-7-O-Neohesperidoside (Neodiosmin)*	Flavonoids	Flavones	C28H32O15	609.18	301.08	608.1741	[M+H]+	32524972	32358014	36902643
2-(hydroxymethyl)pyridin-3-ol	Alkaloids	Alkaloids	C6H7NO2	126.06	108.05	125.0477	[M+H]+	36329981	33472771	31616620
Diosmetin 7-O-rutinoside	Flavonoids	Flavones	C28H32O15	609.18	301.08	608.1741	[M+H]+	32522086	32168502	35477474
Ethylparaben	Phenolic acids	Phenolic acids	C9H10O3	165.06	92.03	166.063	[M-H]-	35052713	29160722	35787807
5-Hydroxymethyl-2-furaldehyde*	Others	Aldehyde compounds	C6H6O3	127.04	53.04	126.0317	[M+H]+	33365271	32433830	32114945
Chrysoeriol-7-O-rutinoside	Flavonoids	Flavones	C28H32O15	607.17	299.05	608.1741	[M-H]-	26309165	34176129	36015489
Phloroglucinol	Others	Others	C6H6O3	127.04	81.03	126.0317	[M+H]+	32283958	31984623	31640103
Swertisin	Flavonoids	Flavones	C22H22O10	447.13	297.08	446.1213	[M+H]+	27185537	27288233	35339638
5-hydroxymethylenefural*	Others	Others	C6H6O3	127.04	53.04	126.0317	[M+H]+	31409951	28974897	28810520
Choline	Alkaloids	Alkaloids	C5H14NO+	104.11	60.08	104.107	[M]+	28278989	27521974	27679419
Kaempferide 3-rutinoside*	Flavonoids	Flavonols	C28H32O15	609.18	301.07	608.1741	[M+H]+	23986921	22796460	35773096
Acacetin-7-O-rutinoside (Linarin)*	Flavonoids	Flavones	C28H32O14	593.19	285.08	592.1792	[M+H]+	26452144	22435014	31940978
7-Methoxy-3-[1-(3-pyridyl)methylidene]-4-chromanone	Flavonoids	Other Flavonoids	C16H13NO3	268.1	136.06	267.0895	[M+H]+	24360796	25230773	26692720
Peonidin-3-O-(6"-O-p-coumaroyl)glucoside	Flavonoids	Anthocyanidins	C31H29O13+	609.16	301.07	609.1603	[M]+	23855657	18004875	27077349
4-amino-2-methylbutanoic acid*	Alkaloids	Alkaloids	C5H11NO2	118.09	58.07	117.079	[M+H]+	22304182	21336466	21119946
Zarzissine	Alkaloids	Alkaloids	C5H5N5	136.06	119.04	135.0545	[M+H]+	22907584	18949016	22246549
Betaine*	Alkaloids	Alkaloids	C5H11NO2	118.09	58.07	117.079	[M+H]+	22228385	20381392	21364825
2-Decanol*	Others	Alcohol compounds	C10H22O	157.16	157.16	158.1671	[M-H]-	20564441	21224592	21636332
6α,10α-Dihydroxy-1-oxoeremophila-7(11),8(9)-dien-12,8-olide	Terpenoids	Sesquiterpenoids	C15H18O5	279.12	149.02	278.1149	[M+H]+	20883591	18954859	19591552
3-Hydrocinnamyl-6-CinnamylGlucose	Others	Alcohol compounds	C24H30O6	415.21	119.09	414.2042	[M+H]+	16349112	29917806	12936997

2,5-O-Di-CinnamylSorbitol	Phenolic acids	Phenolic acids	C24H30O6	415.21	119.09	414.2042	[M+H]+	17901629	28273491	11891717
4'-Demethyleucomin glucosyl rhamnoside*	Flavonoids	Other Flavonoids	C28H32O14	593.18	285.08	592.1792	[M+H]+	18045712	16481609	22366638
Lidocaine	Alkaloids	Alkaloids	C14H22N2O	235.18	86.1	234.1732	[M+H]+	18731872	19617289	17823836
Acacetin-7-O-neohesperidoside*	Flavonoids	Flavones	C28H32O14	593.19	285.08	592.1792	[M+H]+	17402692	14853821	22304277
3-Chloroaniline	Alkaloids	Alkaloids	C6H6ClN	128.03	93.06	127.0189	[M+H]+	17084174	17099828	20313282
4-Hydroxybenzoate	Phenolic acids	Phenolic acids	C7H6O3	137.02	93.03	138.0317	[M-H]-	19458978	15523474	18795881
Dibutyl phthalate	Phenolic acids	Phenolic acids	C16H22O4	279.16	149.02	278.1518	[M+H]+	17819947	18720634	16930306
Des-O-Methyllasiodiplodin	Others	Lactones	C16H22O4	279.16	149.03	278.1518	[M+H]+	17996145	17414390	17792530
7-{[(2S,3R,4R,5S,6R)-3,4-dihydroxy-6-(hydroxymethyl)-5-{[(2R,3R,4R,5R,6S)-3,4,5-trihydroxy-6-methyloxan-2-yl]oxy}oxan-2-yl]oxy}-5-hydroxy-2-(4-methoxyphenyl)chromen-4-one*	Flavonoids	Flavones	C28H32O14	593.19	285.08	592.1792	[M+H]+	17189483	14262154	21478992
triptobenzene D	Terpenoids	Ditepenoids	C20H26O2	297.18	297.18	298.1933	[M-H]-	18396096	13847323	17575344
2-Methylpyrrolidine-2-carboxylic acid	Alkaloids	Alkaloids	C6H11NO2	130.09	84.09	129.079	[M+H]+	16547912	16172408	15608534
1-Decanol*	Others	Alcohol compounds	C10H22O	157.16	157.16	158.1671	[M-H]-	14764753	15441061	16413551
3,4-Dihydroxybenzaldehyde	Others	Aldehyde compounds	C7H6O3	137.02	93.04	138.0317	[M-H]-	15680772	14316842	16494649
N-(3-hydroxy-4-methoxyphenethyl)-4-hydroxybutanamide	Alkaloids	Alkaloids	C14H21NO4	268.15	136.06	267.1471	[M+H]+	15202246	14945783	15237357
Lauryldiethanolamine	Others	Others	C16H35NO2	274.28	88.08	273.2668	[M+H]+	14232286	13305054	13816417
Chrysoeriol-6-C-rhamnoside-7-O-rhamnoside	Flavonoids	Flavones	C28H32O14	593.18	447.13	592.1792	[M+H]+	13781142	9760379.2	14512549
Phyllanthusiin E	Others	Others	C13H8O8	291.01	247.03	292.0214	[M-H]-	11812246	10635809	15140620
1,2,3,4-Tetrahydro-3-carboxy-2-carboline	Alkaloids	Alkaloids	C12H12N2O2	217.1	144.08	216.0899	[M+H]+	12051354	11335894	14006184
Norephedrin 3-O-(2"-Phenylpropanyl)Glucoside	Alkaloids	Phenolamine	C24H33NO6	432.24	119.09	431.2308	[M+H]+	11219128	17125932	8220743.7

6-Demethoxy-4'-O-methylcapillarisin rhamnosyl glucoside	Others	Chromone	C28H32O15	607.16	299.06	608.1741	[M-H]-	11885772	10067873	14170398
8-(5-Hydroxy-2,6,6-Trimethylcyclohex-2-En-1-Yl)-6-Methyloct-5-En-2-one	Terpenoids	Sesquiterpenoids	C18H30O2	279.23	81.07	278.2246	[M+H]+	13304099	8701393.4	12724689
9-hydroxy-8-{[(2S,3R,4S,5S,6R)-3,4,5-trihydroxy-6-(hydroxymethyl)oxan-2-yl]oxy}-1H,3H-naphtho[2,3-c]furan-1-one	Others	Others	C18H18O9	377.09	341.11	378.0951	[M-H]-	11595587	10952868	11708653
Tanaphillin	Terpenoids	Sesquiterpenoids	C15H18O5	279.12	149.02	278.1154	[M+H]+	10910552	10889169	12213310
2,6-Dimethyl-7-octene-2,3,6-triol	Terpenoids	Monoterpenoids	C10H20O3	187.13	97.06	188.1412	[M-H]-	11149188	11447867	11389462
8,10-Diethyllobelionol	Alkaloids	Piperidine alkaloids	C14H27NO2	242.22	170.15	241.2042	[M+H]+	11283203	10173765	10575193
Sulfo jasmonate	Others	Others	C12H18O7S	305.07	96.96	306.0773	[M-H]-	8658722	11472677	11350265
2-Piperidone	Alkaloids	Piperidine alkaloids	C5H9NO	100.08	56.05	99.0684	[M+H]+	10925922	10634282	9890080.8
Inokosterone*	Steroids	Steroid	C27H44O7	481.32	445.3	480.3087	[M+H]+	9170516.7	10674071	11239035